KELL s.r.l.
Via E.Q. Visconti, 8
00193 Roma
tel. 06 36004916
fax 06 3216937
www.kell.it

.....

n.i. e partita iva
05419421002
R.E.A. n°887680
cap. soc. €. 10.400,00
Sede legale
Via Plinio, 22 00193 Roma

AIRFIRE

Final Report

ESA contract C/N 20090

GALILEO AVIONICA
Una Società Finmeccanica

Doc. Ref.	AIRFIRE-FIN-01
Issue:	
Status	
Date	22/10/2007
Authors	Agostino Fiorani, Antonella Canestro, Fabrizio Aversa Stefania Amici, Valerio Lombardo
Checked	Fabrizio Aversa
Project Manager	Fabrizio Aversa

Document Change Log

Issue	Date	Reason for change
1	22/10/2007	First Issue

Reference Documents

Name	Issue	Date	Title
AIRFIRE-CRR	1	02/08/2006	Campaign Readiness Report
AIRFIRE-DAR-02	1	15/11/2006	AIRFIRE - Data Acquisition Report
Dozier		RSE 1981	A method for satellite identification of surface temperature fields of subpixel resolution
E. Cisbani et al		IGARSS 2002	Early fire detection system based on multi-temporal images of geostationary and polar satellites
Vodacek, A., R.L. Kremens, A.J. Fordham, S.C. VanGorden et al.		2002	Remote optical detection of biomass burning using a potassium emission signature. Int. J. Remote Sens. 23:2721-2726 .

TABLE OF CONTENTS

1 Introduction

The idea that spaceborne instruments on polar and geostationary satellites can help in wildfire detection and monitoring is well consolidated in the remote sensing community (see for ex. Y. Kaufman, Justice C., Flynn, L. Kendall J., Prins. E, Giglio L., Ward D.E.,Menzel P. and A. Setzer, "Potential Global Fire Monitoring from EOS – MODIS", *J.Geoph. Res, -Atmosphere* 103 (1998) 32215-32238, and E. Cisbani et al., "Early fire detection system based on multi-temporal images of geostationary and polar satellites", *IGARSS 2002*, Toronto, July 2002).
Observations from satellites currently in orbit are made with a ground resolution pixel size that exceeds the majority of wildfires. Therefore, the objective of the campaign was to take high-resolution images of fires from aircraft to act as 'ground truth' data in order to validate present models used for the assessment of products obtained from satellite observations of wildfires.
Tha camapign scope was to validate and assess the results obtainable through the most relevant satellite observation techniques, against the high resolution fire mapping information derived from a dedicated hyperspectral airborne campaign. The result of this analysis shall be reported in terms of requirements for bands, trying to outline a comprehensive approach to fire monitoring services based on satellite data.
The choice of implementing an airborne campaign to produce the data to be used in this assessment and validation process is due to the following reasons:

- aircraft can be at the right place at the right time even in the case of an unpredictable phenomenon like a wildfire;
- available airborne instruments can be tuned and offer the large spectral coverage needed for a global analysis;
- aerial surveys can produce high quality, high resolution fire mapping data to be used as "ground truth" data required for the assessment and validation of the results obtained from satellite observations of wildfires.

The campaign was carried out during August 2006 over the Tuscan and Lazio regions in Italy. The time and place for the campaign was chosen to tie in with the high probability of finding wildfires in an area that the team could quickly reach by light aircraft.The campaign has been performed employing two aircraft:

- An AS-350 (I-AMLT) twin engine helicopter, equipped with an AGEMA 1000 IR camera maounted on a gyro-stabilized Wescam platform
- An Allegro 2000 Ultralight aircraft (I-7886) equipped with the Selex SAS SIM-GA hyperspectral sensor.

The AS-350 is normally dedicated to TV broadcasting and law enforcement activities. The ultralight aircraft is a flying platform for several sensors and telecommunication devices, operated by Kell Avio, that is hired by Kell for this activity.

1.1 SIG-MA HYPER Sensor

The SIG-MA HYPER developed by Selex SAS is a modular avionic hyperspectral system, mainly composed of two electrooptical heads (EOH) in VNIR and SWIR spectral range (from 0.4 mm to 2.5 mm) and a digital acquisition system. This instrument is one of the components of SIM.GA system (Sistema Iperspettrale Multisensoriale – Galileo Avionica) that will include four hyperspectral / multispectral optical heads (VNIR, SWIR, MIR and TIR) providing a spectral coverage from visible band (0.4 mm) to thermal infrared (12 mm) band.
The two EOHs are physically separated but placed side by side on a common alignment plate and enclosed in a protecting box.The "modular" approach allows, with just a change of mechanical interface, a flexible arrangement of instrument accommodation and therefore the possibility of its use on small platforms (including UAVs and ultralight aircrafts). A "pushbroom" scanning mode (looking at nadir) is used to acquire the spectral data cube. To derive geo-registered images the flight data coming from a dedicated GPS/INS unit are logged continuously.
The technical characteristics of the instrument are summarized in the following table.

	VNIR Channel		SWIR Channel	
Spectral Range	400-1000 nm		1000-2500 nm	
Spectral Sampling	≈ 1.2 nm		≈ 5.8 nm	
# Spectral sampling	500		256	
# Spatial Pixels	1024		320	
Focal Lenght (*)	24 mm	17 mm	22.5 mm	30.7 mm
Nominal IFOV per pixel	0.5 mrad	0.7 mrad	1.3 mrad	1 mrad
Spatial resolution @ 1000 m	0.5 m	0.7 m	1.3 m	1 m
Swath @ 1000 m	512 m	715 m	415 m	320 m
FOV	± 14 °	± 19°	± 12 °	± 9.0 °
F#	2.0		2.0	
Quantization Bits	12 bits		14 bits	
Detector	Camera CCD		CMT cooled at 200 K	
Maximum frame rate	57 fps		100 fps	
Weight	25 Kg			
Power (peak)	16 W		250 W	

1.2 TIR Sensor

The IR camera is an AGEMA THV 1000 in the helicopter arrangement.
It operates in the 8-12 micron range, with a FOV of 5.0 x 3.3 deg or 20.0 x 13.0 deg and 800 sample lines.
It was be able to record temperatures in the range -20 to 115 centigrades.
The camera is mounted in a 16" Wescam gyro-stabilized certified platform on the helicopter.
The images supplied by the camera report a color scale corresponding to a temperature. The temperature range is configurable during operations.

On July 28th 2006 the system has been integrated, the qualification flight acquiring the first data-sets performed and the campaign started.

The following picture shows the aircraft flying with the instrument taking data.


I-7886

2 Level 1 data processing

2.1 Level1 data reading and deformatting

2.1.1 Hyper data processing

The Hyper data analysis consists of different steps. The first phase is a quick look of the data in order to select the "good data" and point out any problem that can affect the other steps The second phase is named data pre-processing and consists of the geometrical correction, geocoding and data calibration. The third phase is the product generation and result evaluation (Figure 2-1)

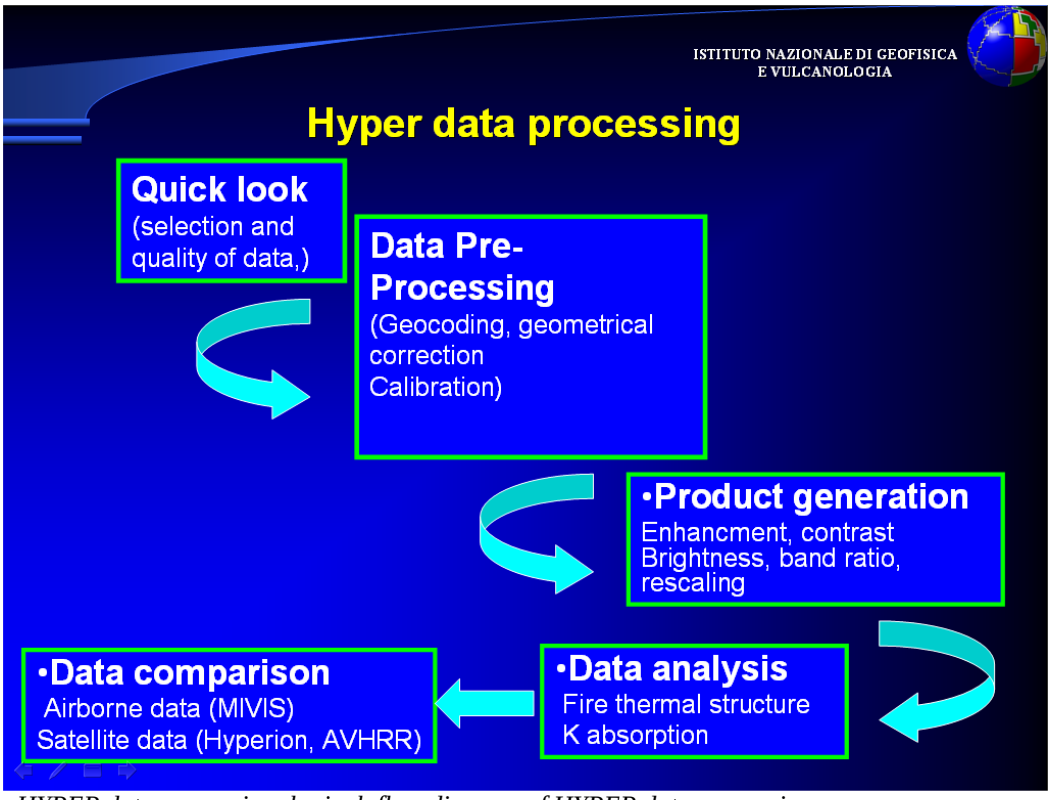

Figure 2-1- *HYPER data processing logical flow diagram of HYPER data processing.*

2.1.2 Hyper data

Table 2-1 shows the days during which data were acquired in correspondence of different kind of fires.

Date	Interested area
2006/08/02	Test fly
2006/08/04	Centrale Montalto Campagnano e Soratte 02:30 hours
2006/08/08	Cesano 00:30 hours
2006/08/09	gps failure 01:00 hour
2006/08/10	GPS log .pdf 01:00 hour
2006/08/14	Magliano/Campagnano Misto vegetazione bassa e alta Manziana/Oriolo, un gruppo di alberi con fiamme alte senza operazioni di spegnimento. 02:00 hours
2006/08/15	post fire (14/08) 01:00 tempo volo
2006/08/16	Nemi (Frascati) 01:30 hours
2006/08/19	Cerveteri 01:00 hours
2006/8/20	Magliano/Campagnano 01:00 hours

Table 2-1

A quick look of data has been realized in order to select the data set to be processed.

The criteria followed for the selection were quality of data, level of noise, saturation, scientific interest of the acquired data, typology of vegetation. The quick look allowed to add some comments and information useful for the analysis**.**

Date	Area	Filename	Tint [ms]	GPS	Sample	Line	Comments
2006/08/14	Magliano Campagnano	20060814T160326_SWIR_DARK-0.raw	10	Data82log.log	320	251	
2006/08/14	Magliano Campagnano	20060814T160326_VNIR_DARK_0.raw	16	Data82log.log	1024	507	
2006/08/14	Magliano Campagnano	20060814T160436_SWIR_DARK_0.raw	10	Data82log.log	320	62	
2006/08/14	Magliano Campagnano	20060814T160436_VNIR_DARK_0.raw	16	Data82log.log	1024	145	
2006/08/14	Magliano Campagnano	20060814T160803_SWIR_DARK_0.raw	10	Data82log.log	320	120	
2006/08/14	Magliano Campagnano	20060814T160802_VNIR_DARK_0.raw	16	Data82log.log	1024	255	
2006/08/14	Magliano Campagnano 42° 08’ 26.873” – 12° 25’ 03.288”	20060814T161027_SWIR_0.raw	10	Data82log.log	320	2561	
2006/08/14	Magliano Campagnano 42° 08’ 26.873” – 12° 25’ 03.288	20060814T161026_VNIR_0.raw	16	Data82log.log	1024	2000	Burned area
2006/08/14	Magliano Campagnano	20060814T161026_VNIR_1.raw	16	Data82log.log	1024	2000	

Date	Area	Filename	Tint [ms]	GPS	Sample	Line	Comments
	42° 08' 26.873" – 12° 25' 03.288						
2006/08/14	Magliano Campagnano 42° 08' 26.873" – 12° 25' 03.288	20060814T161026_VNIR_2.raw	16	Data82log.log	1024	930	smoke
2006/08/14	Magliano Campagnano	20060814T161729_SWIR_0.raw	10	Data82log.log	320	528	noisy
2006/08/14	Magliano Campagnano	20060814T161729_VNIR_0.raw	16	Data82log.log	1024	1035	fires
2006/08/14	Magliano Campagnano	20060814T161858_SWIR_0.raw	10	Data82log.log	320	1618	
2006/08/14	Magliano Campagnano	20060814T161857_VNIR_0.raw	16	Data82log.log	1024	2000	Fires smoky
2006/08/14	Magliano Campagnano : 42° 08' 40.729" – 12° 27' 20.009"	20060814T161857_VNIR_1.raw	16	Data82log.log	1024	1124	Fire and smoke
2006/08/14	Magliano Campagnano	20060814T162721_SWIR_0.raw	5	Data82log.log	320	1699	Front and smoke
2006/08/14	Magliano Campagnano	20060814T162721_VNIR_0.raw	16	Data82log.log	1024	2000	
2006/08/14	Magliano Campagnano	20060814T162721_VNIR_1.raw	16	Data82log.log	1024	1280	Front fire
2006/08/14	Magliano Campagnano	20060814T163046_SWIR_0.raw	2	Data82log.log	320	1986	Front fire smooth
2006/08/14	Magliano Campagnano	20060814T163046_VNIR_0.raw	16	Data82log.log	1024	2000	
2006/08/14	Magliano Campagnano	20060814T163046_VNIR_1.raw	16	Data82log.log	1024	1826	Front fire smooth
2006/08/14	Magliano Campagnano 42°08' 1.41" 12°25'50.237"	20060814T163334_SWIR_0.raw	2	Data82log.log	329	1362	Front fire smooth
2006/08/14	Magliano Campagnano	20060814T163333_VNIR_0.raw	16	Data82log.log	1024	2000	Front fire
2006/08/14	Magliano Campagnano	20060814T163333_VNIR_1.raw	16	Data82log.log	1024	634	Front and smoke
2006/08/14	Magliano Campagnano 42° 08' 41.641" – 12° 25' 50.237"	20060814T163804_VNIR_DARK_0.raw	16	Data82log.log	1024	156	
2006/08/14	Magliano Campagnano 42° 08' 41.641" – 12° 25' 50.237"	20060814T163804_SWIR_DARK_0.raw	1	Data82log.log	320	68	
2006/08/14	Magliano Campagnano	20060814T164111_SWIR_0.raw	1	Data82log.log	320	1852	front fire
2006/08/14	Magliano Campagnano	20060814T164110_VNIR_0.raw	16	Data82log.log	1024	2000	village
2006/08/14	Magliano Campagnano	20060814T164110_VNIR_1.raw	16	Data82log.log	1024	1572	
2006/08/14	Magliano Campagnano	20060814T164438_SWIR_0.raw	1	Data82log.log	320	2675	Front fire
2006/08/14	Magliano Campagnano	20060814T164438_VNIR_0.raw	16	Data82log.log	1024	2000	village
2006/08/14	Magliano Campagnano	20060814T164438_VNIR_1.raw	16	Data82log.log	1024	2000	smoke
2006/08/14	Magliano Campagnano	20060814T164438_VNIR_2.raw	16	Data82log.log	1024	1147	Front fire
2006/08/14	Magliano Campagnano	20060814T165254_SWIR_0.raw	0.5	Data82log.log	320	1208	Front fire

Date	Area	Filename	Tint [ms]	GPS	Sample	Line	Comments
2006/08/14	Magliano Campagnano	20060814T165254_VNIR_0.raw	16	Data82log.log	1024	2000	Smoke
2006/08/14	Magliano Campagnano	20060814T165254_VNIR_1.raw	16	Data82log.log	1024	338	Fire and smoke
2006/08/14	Magliano Campagnan	20060814T171049_SWIR_DARK_0.raw	2	Data82log.log	320	37	
2006/08/14	Magliano Campagnano	20060814T171049_VNIR_DARK_0.raw	16	Data82log.log	1024	95	
2006/08/14	Magliano Campagnano	20060814T171254_SWIR_0.raw	2	Data82log.log	320	2394	Front file
2006/08/14	Magliano Campagnano	20060814T171253_VNIR_1.raw	16	Data82log.log	1024	2000	Smoke front
2006/08/14	Magliano Campagnano	20060814T171556_SWIR_0.raw	2	Data82log.log	320	1317	Saturation 1.6 10^4
2006/08/14	Magliano Campagnano	20060814T17156_VNIR_0.raw	16	Data82log.log	1024	2000	Smoke front (saved data)
2006/08/14	Magliano Campagnano	20060814T171556_VNIR_1raw	16	Data82log.log	1024	547	Smoke front (saved data)
2006/08/14	Oriolo	20060814T171750_SWIR_0.raw	2	Data82log.log	320	1400	Front
2006/08/14	Oriolo	20060814T171750_VNIR_0.raw	16	Data82log.log	1024	2000	
2006/08/14	Oriolo	20060814T172128_SWIR_0.raw	2	Data82log.log	320	1372	Front
2006/08/14	Oriolo	20060814T172128_VNIR_0.raw	16	Data82log.log	1024	2000	Front
2006/08/14	Oriolo	20060814T172128_VNIR_1.raw	16	Data82log.log	1024	652	
2006/08/14	Oriolo	20060814T173443_SWIR_DARK_0.raw	4	Data82log.log	320	135	
2006/08/14	Oriolo	20060814T173443_VNIR_DARK_0.raw	16	Data82log.log	1024	282	
2006/08/14	Oriolo	20060814T173642_SWIR_0.raw	4	Data82log.log	320	1657	Front
2006/08/14	Oriolo	20060814T173642_VNIR_1.raw	16	Data82log.log	1024	1198	Front
2006/08/14	Oriolo	20060814T173844_SWIR_0.raw	4	Data82log.log	320	1735	Front e ghost
2006/08/14	Oriolo	20060814T173844_VNIR_0.raw	16	Data82log.log	1024	2000	Only smoke
2006/08/14	Oriolo	20060814T173844_VNIR_1.raw	16	Data82log.log	1024	1347	Front
2006/08/14	Oriolo	20060814T174050_SWIR_0.raw	4	Data82log.log	320	1168	fire
2006/08/14	Oriolo	20060814T174050_VNIR_0.raw	16	Data82log.log	1024	2000	
2006/08/14	Oriolo	20060814T173844_VNIR_1.raw	16	Data82log.log	1024	264	smoke
2006/08/15	Post flame	20060815T152035_SWIR_DARK_0.raw	10	Data82log.log	320	130	
2006/08/15	Post flame	20060815T152034_VNIR_DARK_0.raw	16	Data82log.log	1024	274	
2006/08/15	Post flame	20060815T152345_SWIR_0.raw	10	Data82log.log	320	1899	
2006/08/15	Post flame	20060815T152345_VNIR_1.raw	16	Data82log.log	1024	1662	Burned front,
2006/08/15	Post flame	20060815T152615_SWIR_0.raw	10	Data82log.log	320	1396	Burned front,
2006/08/15	Post flame	20060815T152614_VNIR_1.raw	16	Data82log.log	1024	699	
2006/08/16	Nemi	20060816T163841_SWIR_DARK_0.raw	2	Data82log.log	320	143	
2006/08/16	Nemi	20060816T163841_VNIR_DARK_0.raw	16	Data82log.log	1024	298	
2006/08/16	Nemi	20060816T165552_SWIR_0.raw	2	Data82log.log	320	908	Flame, fire, smoke
2006/08/16	Nemi	20060816T165551_VNIR_0.raw	16	Data82log.log	1024	1764	Flame, fire, smoke
2006/08/16	Nemi	20060816T170102_SWIR_0.raw	2	Data82log.log	320	782	
2006/08/16	Nemi	20060816T170102_VNIR_0.raw	16	Data82log.log	1024	1523	
2006/08/19	Cerveteri	20060819T151930_SWIR_0.raw	1	Data82log.log	320	747	Flame front, smoke
2006/08/19	Cerveteri	20060819T151930_VNIR_0.raw	16	Data82log.log	1024	1455	
2006/08/19	Cerveteri	20060819T152047_SWIR_DARK_0.raw	1	Data82log.log	320	147	
2006/08/19	Cerveteri	20060819T152047_VNIR_DARK_0.raw	16	Data82log.log	1024	306	
2006/08/19	Cerveteri	20060819T152114_SWIR_DARK_0.raw	0.2	Data82log.log	320	90	
2006/08/19	Cerveteri	20060819T152114_VNIR_DARK_0.raw	16	Data82log.log	1024	197	
2006/08/19	Cerveteri	20060819T152307_SWIR_0.raw	0.2	Data82log.log	320	1656	Lateral fire
2006/08/19	Cerveteri	20060819T152307_VNIR_1.raw	16	Data82log.log	1024	1197	

Date	Area	Filename	Tint [ms]	GPS	Sample	Line	Comments
2006/08/19	Cerveteri	20060819T152504_SWIR_DARK_0.raw	2	Data82log.log	320	63	
2006/08/19	Cerveteri	20060819T152504_VNIR_DARK_0.raw	16	Data82log.log	1024	147	
2006/08/19	Cerveteri	20060819T152718_SWIR_0.raw	2	Data82log.log	320	1277	
2006/08/19	Cerveteri	20060819T152718_VNIR_0.raw	16	Data82log.log	1024	2000	Burned area
2006/08/19	Cerveteri	20060819T152718_VNIR_1.raw	16	Data82log.log	1024	471	
2006/08/19	Cerveteri	20060819T153347_SWIR_DARK_0.raw	0.2	Data82log.log	320	249	
2006/08/19	Cerveteri	20060819T153347_VNIR_DARK_0.raw	16	Data82log.log	1024	501	
2006/08/20	Magliano Campagnano	20060820T144327_SWIR_DARK_0.raw	3	Data82log.log	320	116	
2006/08/20	Magliano Campagnano	20060820T144327_VNIR_DARK_0.raw	16	Data82log.log	1024	248	
2006/08/20	Magliano Campagnano	20060820T144547_SWIR_0.raw	3	Data82log.log	320	1281	
2006/08/20	Magliano Campagnano	20060820T144547_VNIR_0.raw	16	Data82log.log	1024	2000	
2006/08/20	Magliano Campagnano	20060820T144745_SWIR_0.raw	3	Data82log.log	320	1250	
2006/08/20	Magliano Campagnano	20060820T144744_VNIR_0.raw	16	Data82log.log	1024	2000	
2006/08/20	Magliano Campagnano	20060820T1144854_SWIR_DARK_0.raw	0.5	Data82log.log	320	50	
2006/08/20	Magliano Campagnano	20060820T145032_SWIR_0.raw	0.5	Data82log.log	320	1890	
2006/08/20	Magliano Campagnano	20060820T145032_VNIR_1.raw	16	Data82log.log	1024	1646	
2006/08/20	Magliano Campagnano	20060820T145308_SWIR_0.raw	0.5	Data82log.log	320	1072	Flame front
2006/08/20	Magliano Campagnano	20060820T145307_VNIR_0.raw	16	Data82log.log	1024	2000	
2006/08/20	Magliano Campagnano	20060820T145558_SWIR_0.raw	0.5	Data82log.log	320	683	Burned area of August 14th
2006/08/20	Magliano Campagnano	20060820T145558_VNIR_0.raw	16	Data82log.log	1024	1331	
2006/08/20	Magliano Campagnano	20060820T145819_SWIR_0.raw	0.5	Data82log.log	320	1399	
2006/08/20	Magliano Campagnano	20060820T145818_VNIR_1.raw	16	Data82log.log	1024	704	
2006/08/20	Magliano Campagnano	20060820T150046_SWIR_0.raw	0.5	Data82log.log	320	1116	
2006/08/20	Magliano Campagnano	20060820T150046_VNIR_0.raw	16	Data82log.log	1024	2000	
2006/08/20	Magliano Campagnano	20060820T150517_SWIR_DARK_0.raw	10	Data82log.log	320	52	
2006/08/20		20060820T150516_VNIR_DARK_0.raw	16	Data82log.log	1024	123	
2006/08/20		20060820T151922_SWIR_0.raw	10	Data82log.log	320	1291	Burned area

Table 2-2 - HYPER data quick look results.

Table 2-2 shows HYPER data quick look results. The selected data are summarized according to date and location; comments about the scenes and ancillary information are given.

2.2 Hyper calibration

2.2.1 Calibration processor

In order to express the Hyper DN raw data into physical unit, a calibration processor is needed. The Galileo Avionica provided one calibrated data cube (VIS & SWIR) and calibration factors in order to allow to our processor firstly to reproduce calibrated data and secondly to complete the calibration of HYPER complete data set.
HYPER is an hyperspectral pushbroom sensor that provide "data cube". A data cube is a data that have two spatial facets and a spectral one. The CCD sensor is a 320 spatial pixel (sample) and 256 spectral pixel (bands) for SWIR and 1024 spatial and 516 spectral for VIS. The third spatial direction (line) that completes the cube is of a maximum length of 2000 for both VIS and SWIR. When maximum line is reached a second cube is recorded and a count flag is in the filename is registered.

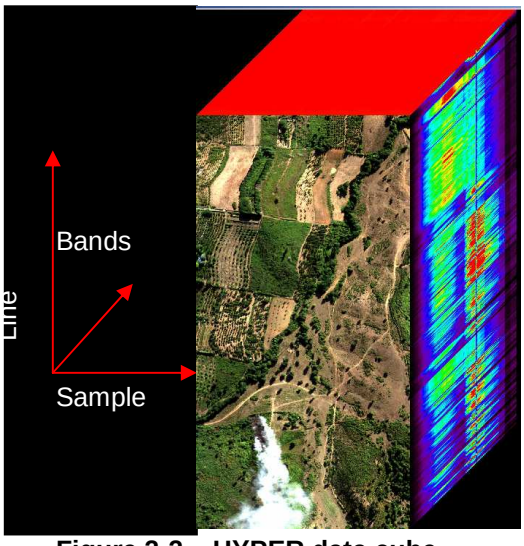

Figure 2-2 – HYPER data cube

The calibration processor has been implemented using IDL for the VIS and SWIR range. We took into account the flat field, the dark current, the integration times and the instrument transfer function measured at laboratory by constructor. The correction for these three functions is applied on each pixel and allow to pass from DN to [W /m2 sr nm].
We used the dark file acquired in the same data acquisition set (not laboratory dark current) for Visible data while for the SWIR we used the laboratory dark current as suggested by Galileo Avionica.
The dark value acquired on flight are very noisy as shown in the Figure 2-3.

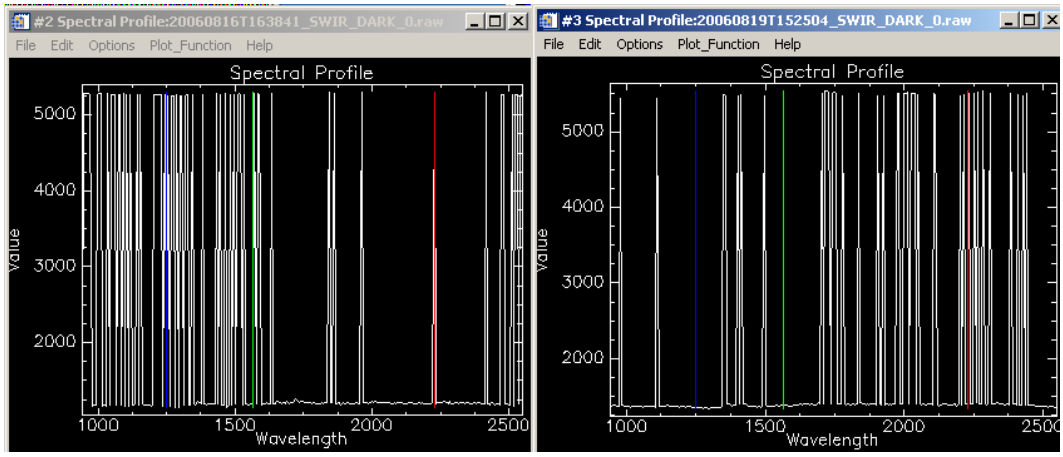

Figure 2-3 – Dark currents

The calibration procedure is semi-automatic: the selection of files is realized by the peak file function while the

algorithm is applied automatically. Data cube is saved in ENVI standard, integer, BIL format. The filename follows the coding as descript in Appendix.

2.2.2 Geometric correction

We tried to adapt an IDL (Interactive Data Language) routine developed for geometric correction of MIVIS data to Hyper data. This procedure has been realized and provided with a graphical user interface, using many routines for image managing/processing provided by the ENVI (the Environment for Visualizing Images) environment. This program requires navigation data as input to generate a displacement map used to correct pixels for non-topographic and topographic deformation.
Non-topographic deformations are due to aircraft movements such as roll, pitch, yaw, bow, etc.
Topographic deformations relate to high variation due to changing topography.

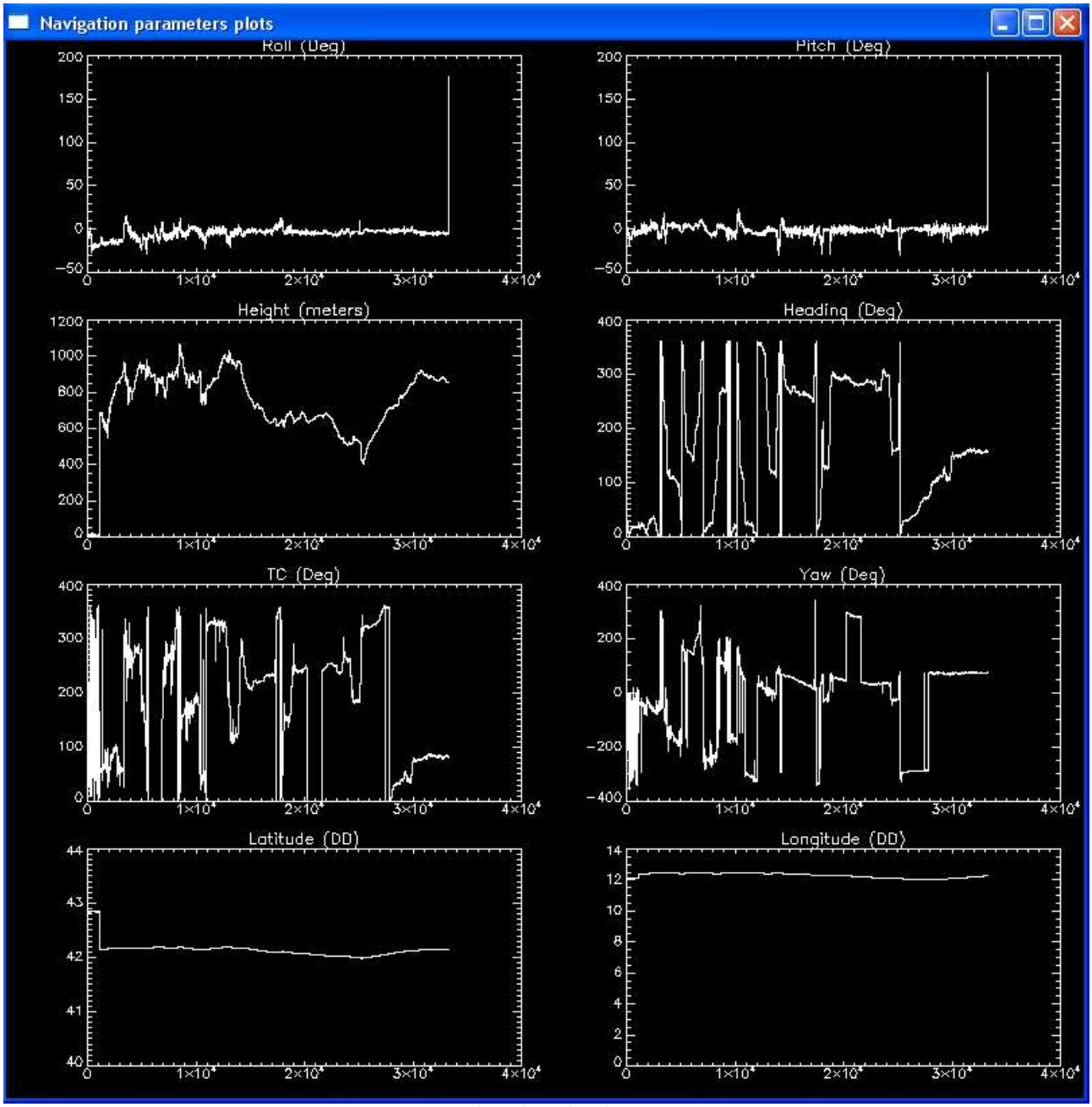

Figure 2-4 - *Plot of navigation parameters*

Unfortunately, there is a big issue outstanding, which is the lacking synchronization between navigation data and recorded images. Therefore is pretty hard to associate correct navigation information to every single line of the image.

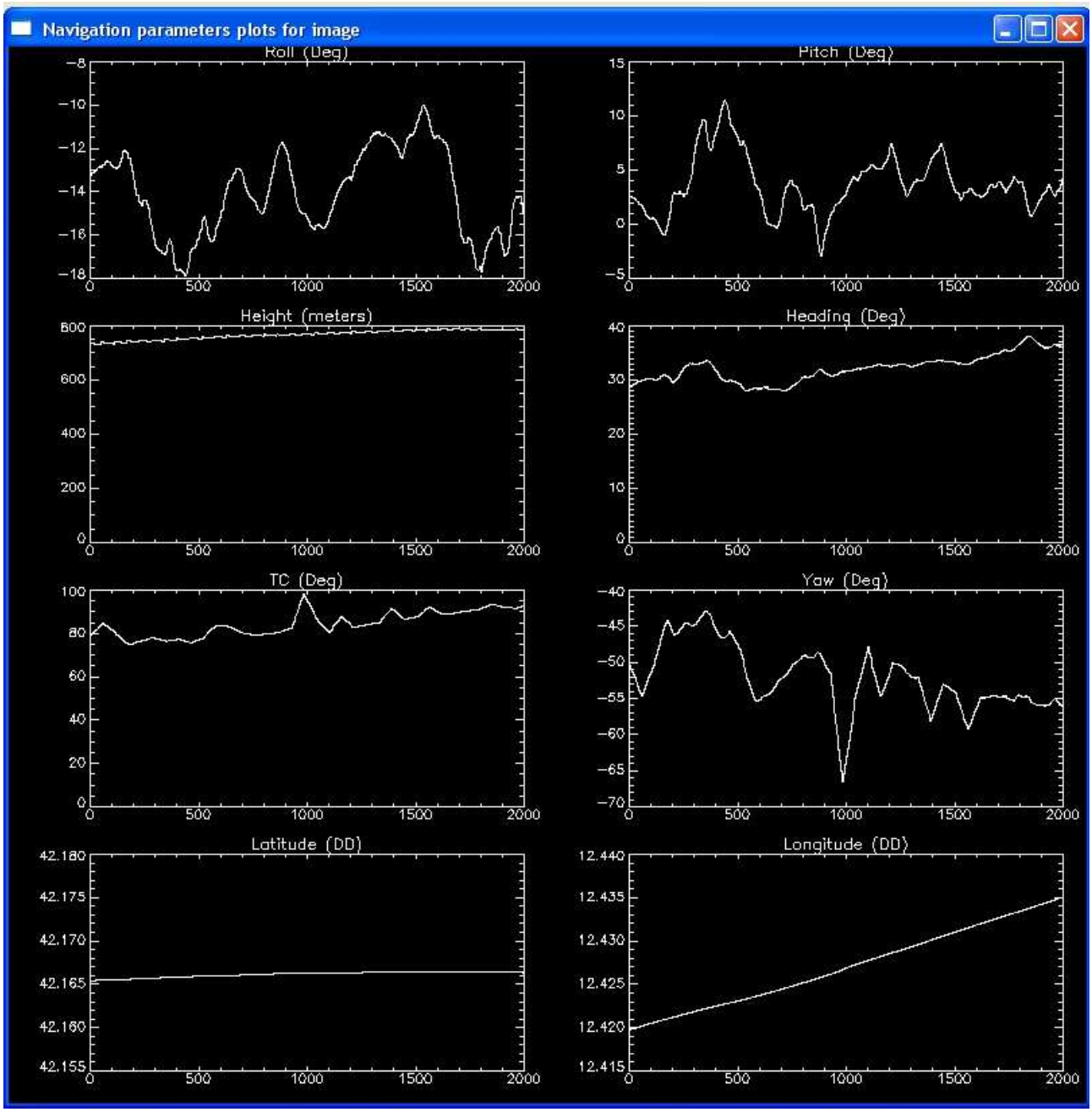

Figure 2-5 - *Plot of navigation parameters assumed to be synchronized with Hyper data*

2.2.3 Semi - automatical correction

The GPS data un position of inertial platform had a sampling frequency lower than the high frequency variation in the shape of the image. With an acquisition rate of 58 Hz, infact 10 pixels are equivalent to ~ 0.17 s 1.5 GPS points. Too few for fit the high frequency oscillation.

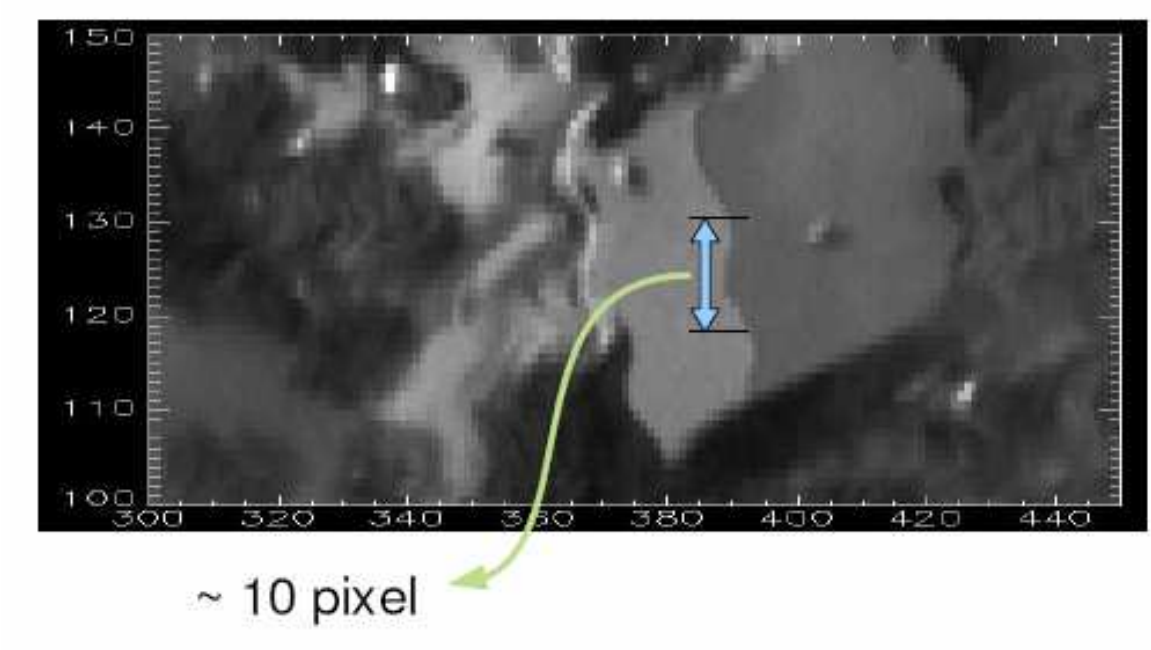

In order to correct high frequency variation in the images a semi automatical procedure has been developed in IDL. In this procedure relevant features (like current cables or houses etc.) can be manually selected and linearized. An example of a result obtained with the procedure is shown in the figure below.

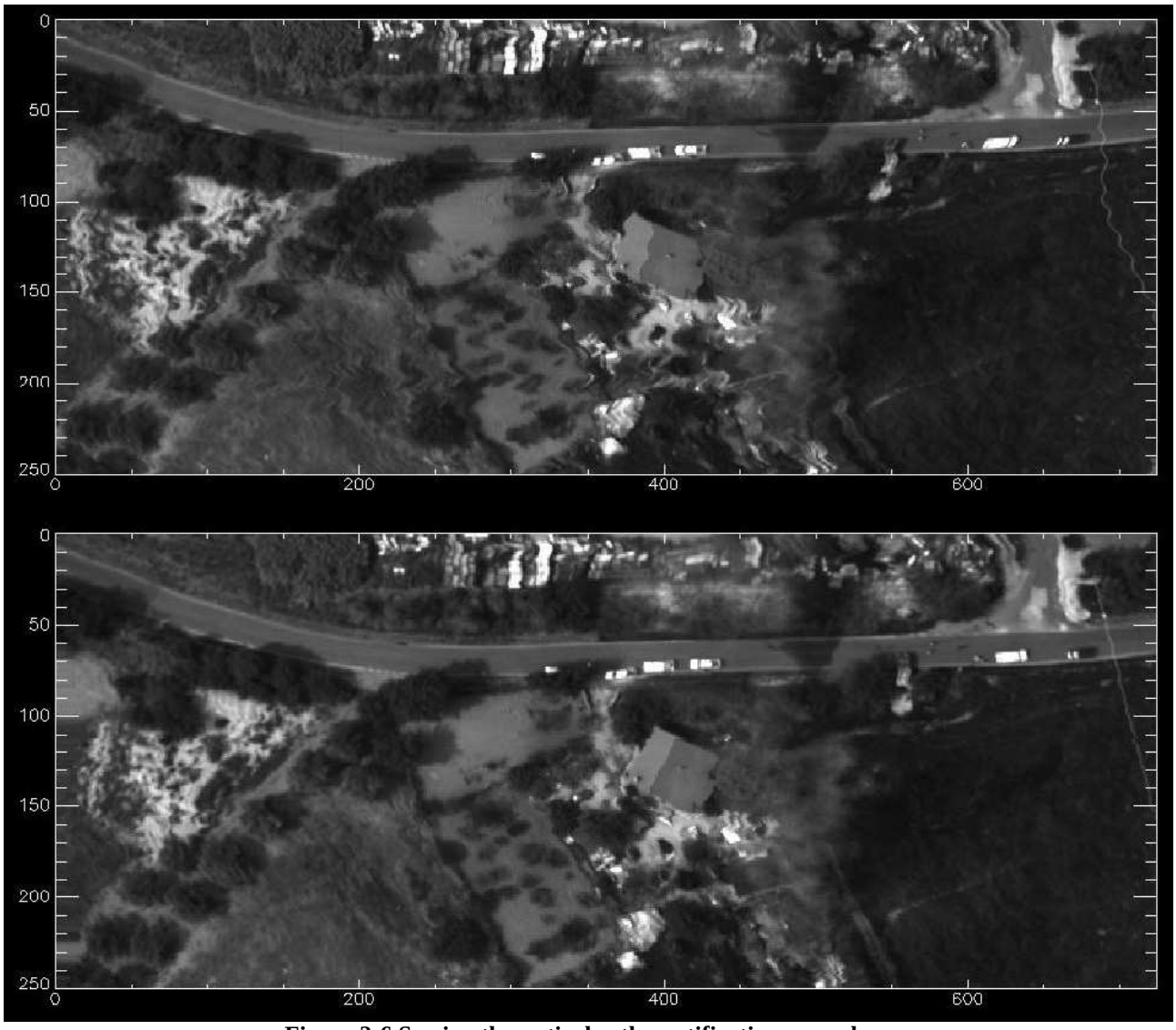

Figure 2-6 Semi authomatical orthorectification procedure

2.2.4 Field Campaign

2.2.4.1 F-Tir

The F-Tir is a detector for measurements collection in the 8-14 mm and 3-5 mm atmospheric windows respectively. Unfortunatly FTIR instrument measurements were not performed due a failure in the temperature control of the instrument.

2.2.4.2 Field Pro spectrometer.

On August 24th 2006, on field measurements have been realized by using the Field Pro spectrometer. The instrument works at 250 - 2500 nm spectral range with a resolution of 3 nm.
The measurements has been carried out on a burned area corresponding to a wild fire (Manziana- Oriolo Romano, N 42 11 48, E 12 10 10) observed by HYPER on August 14th 2006 data

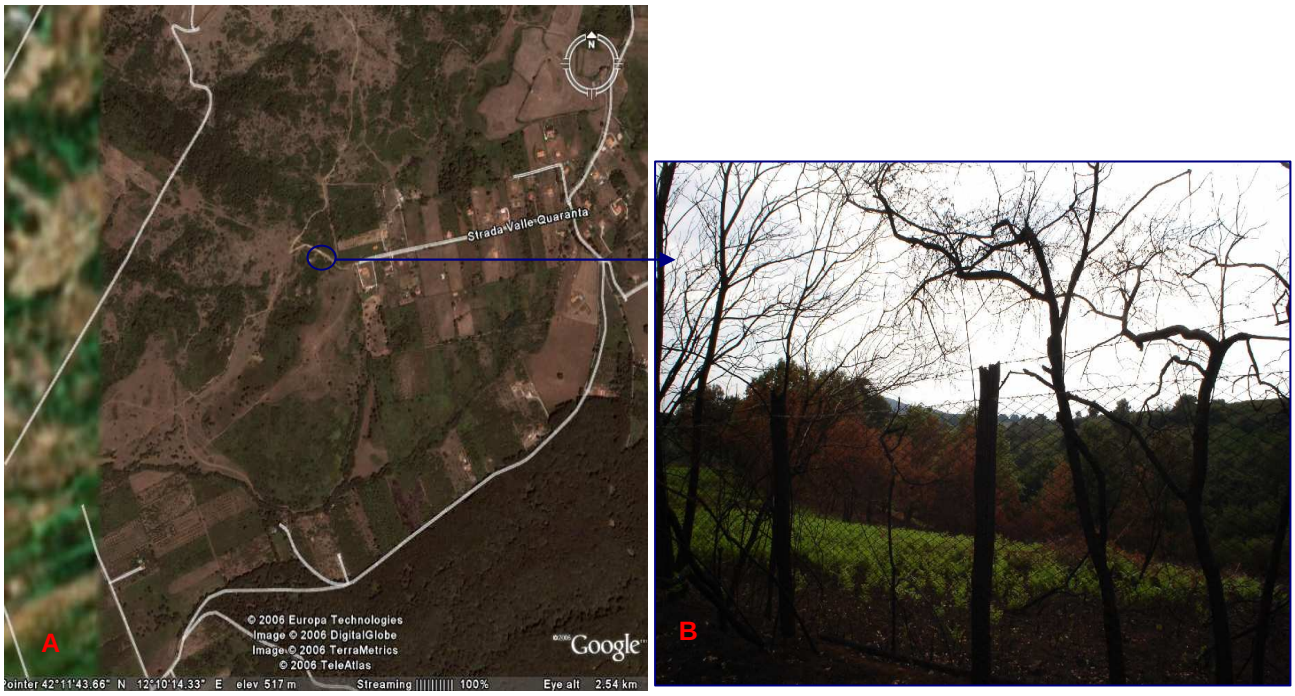

(A) Visible image of the area interested by the wild fire event and (B) the same area 10 days after the event.

The burned area shows some presence of new vegetation growing (fig B). We measured four different kind of samples: ash (A), burned (B), mixture (C) and vegetation and soil (D).
For each kind of samples has been acquired about 50 spectra. Unfortunately during the measurement the weather was cloudy and the measured reflectance show low values.
In the following figures we show an example of the reflectance spectra for each kind of sample.

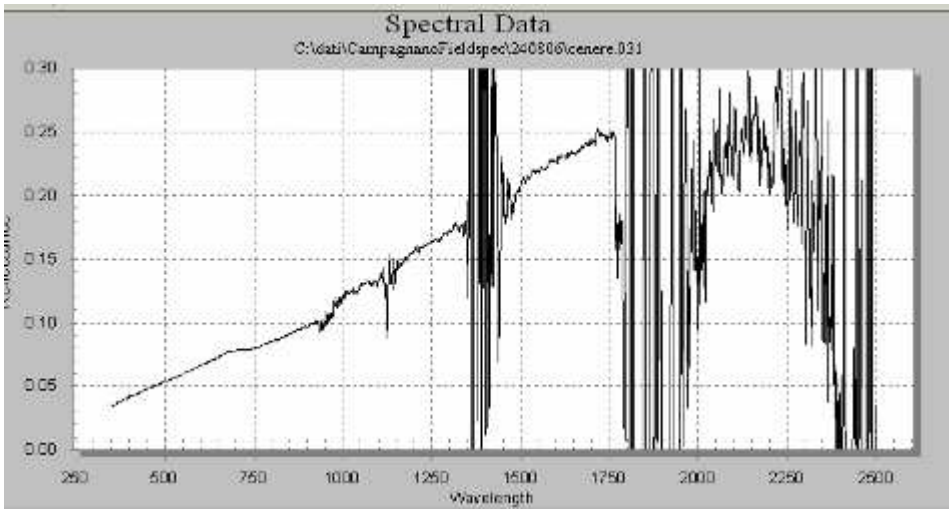

Sample A : ash

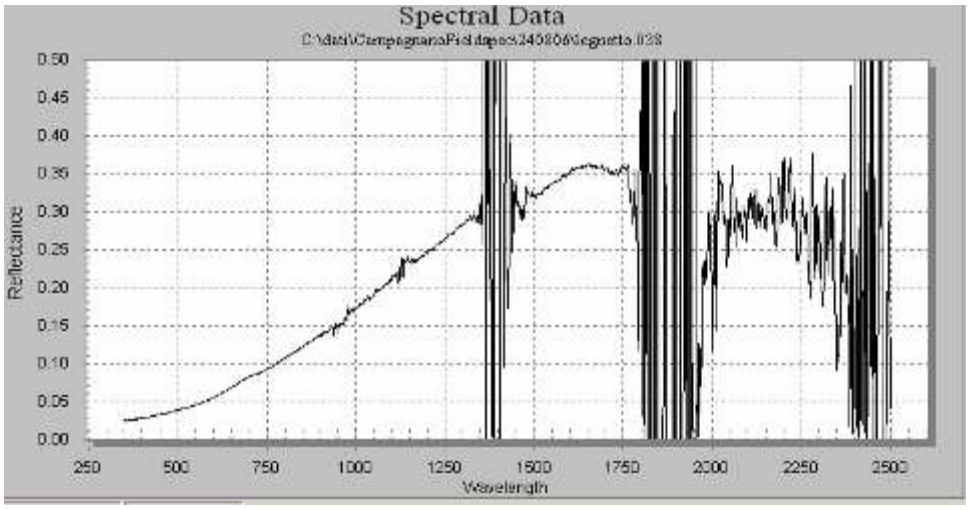

Sample B: burned planking

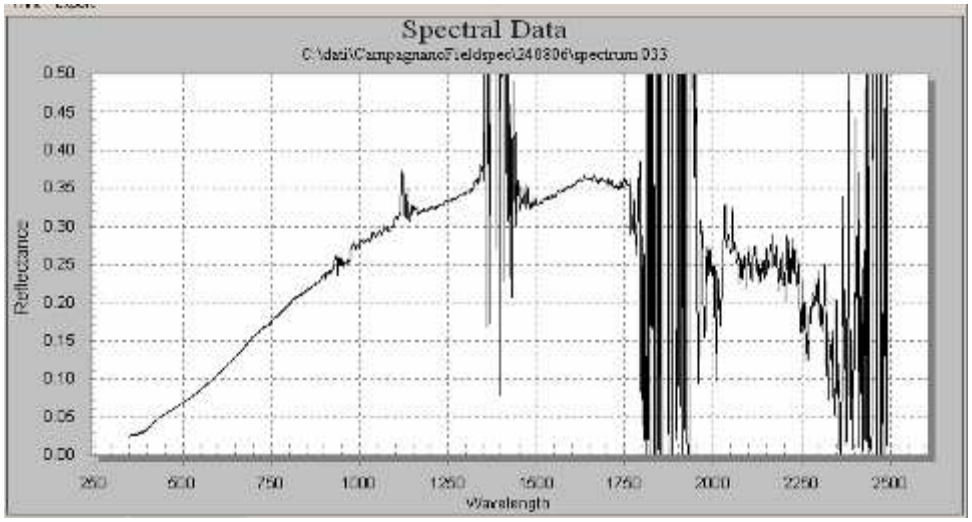

Sample C : mixture

3 Level 2 Campaign data processing

3.1 Data inventory

3.1.1 Selection of data according to different kind of vegetation

We concentrated the analysis on the fire with different kind of vegetation and selected a number of sites to be representative of these categories. The canopy typology was identified on the base of land cover information obtained by the CORINE LAND COVER database of ARPA (Italy).

The overlapping of the land cover map with the Hyper and Google Earth referenced image allowed to identify four different canopy types.

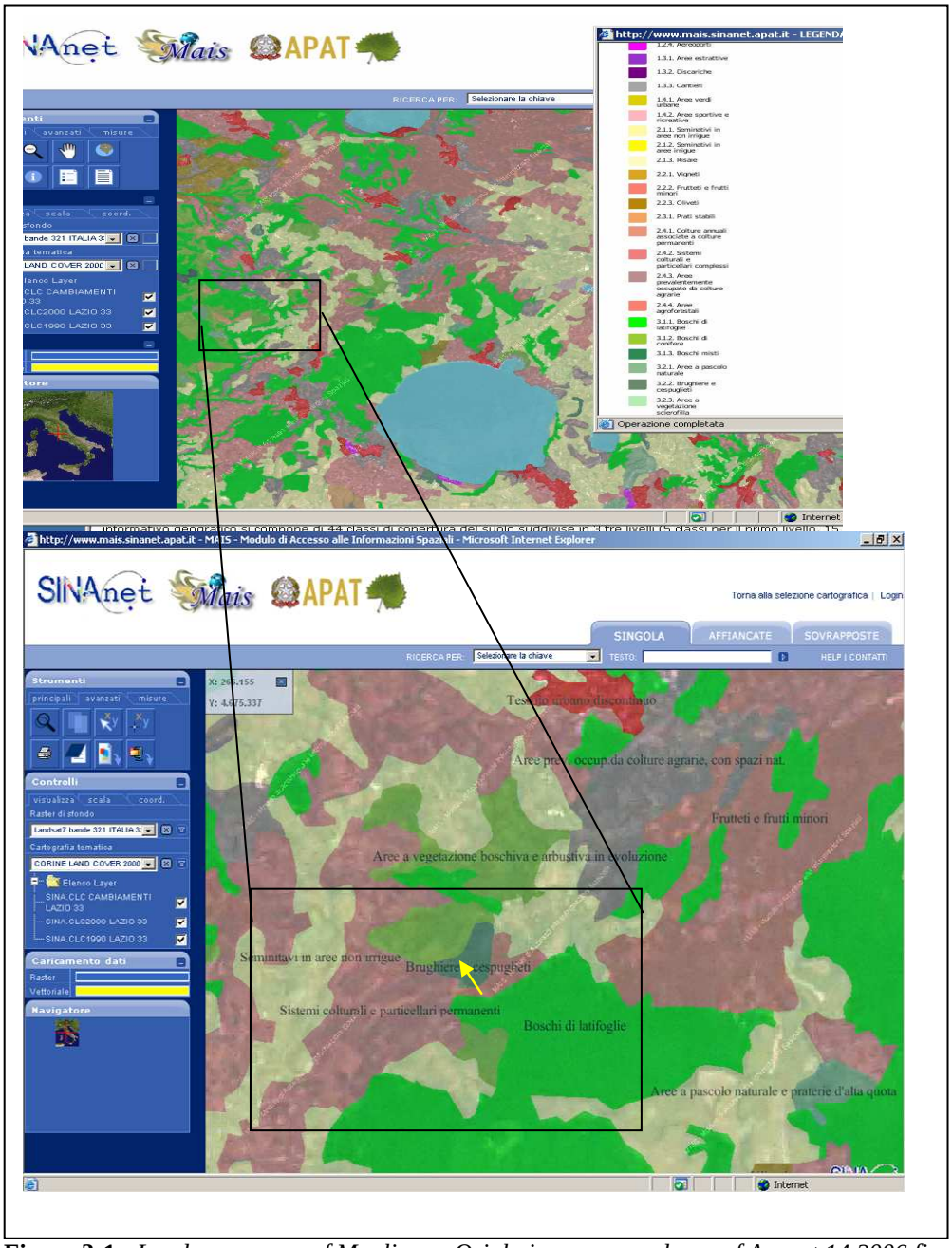

Figure 3-1 - *Land cover area of Magliano –Oriolo in correspondence of August 14 2006 fire*

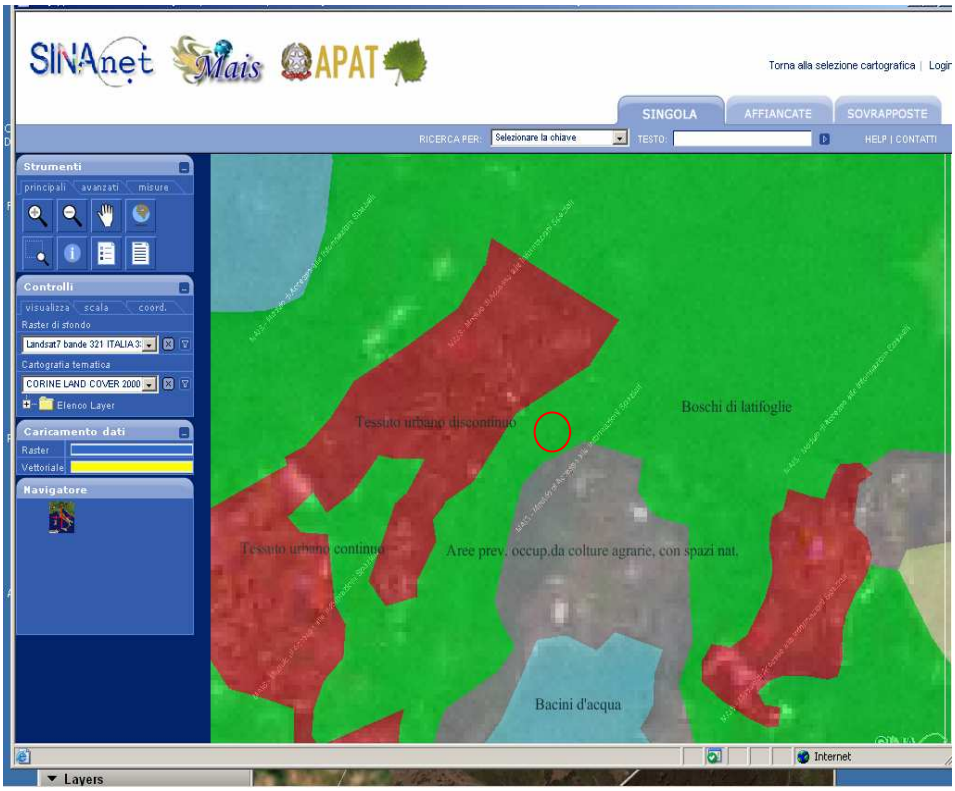

Figure 3-2 *Nemi fire*

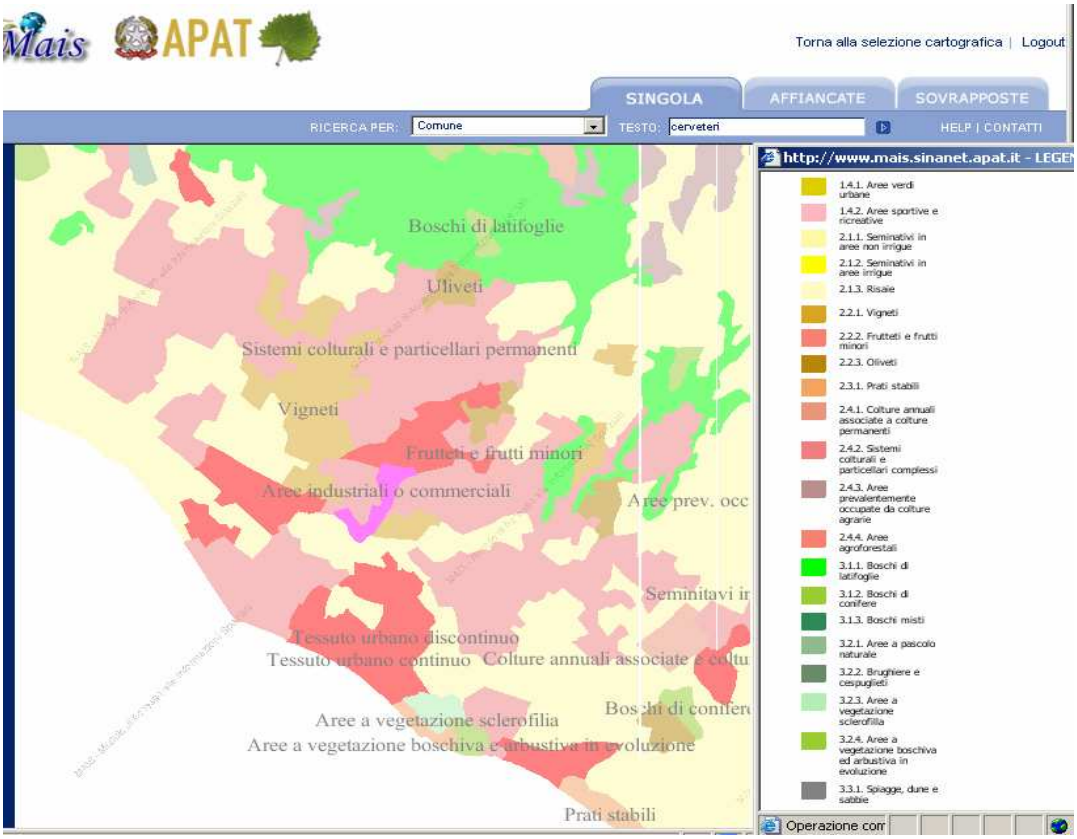

Figure 3.3 *Cerveteri fire land cover*

3.1.2 Data set characterized.

The identification of canopy types allows to selected the data subset to be completely characterized according to the project requirements. In the following table we report the data and the corresponding identified categories.

date	Places	Lat Lon	filename	Categories
	Magliano			Bushes
	Magliano			Bushes
	Magliano			Bushes
2006/08/14	Oriolo	42° 11’ 28.329” – 12° 08’ 47.061	20060814T173642_SWIR_0.raw	Broad-leaved woods
2006/08/14	Oriolo		20060814T173642_VNIR_1.raw	
2006/08/14	Oriolo		20060814T174050_SWIR_0.raw	
2006/08/14	Oriolo		20060814T174050_VNIR_0.raw	
2006/08/16	Nemi	41° 43’ 17.121” 12° 42’ 15.237”	20060816T165552_SWIR_0.raw	Broad-leaved woods
2006/08/16	Nemi	41° 43’ 17.121” – 12° 42’ 15.237”	20060816T165551_VNIR_0.raw	Broad-leaved woods
2006/08/16	Nemi		20060816T170102_SWIR_0.raw	Broad-leaved woods
2006/08/16	Nemi		20060816T170102_VNIR_0.raw	Broad-leaved woods
2006/08/19	Cerveteri	42° 00’ 13.125” – 12° 05’ 12.53”	20060819T152718_SWIR_0.raw	Orchards and and cropped fields
2006/08/19	Cerveteri		20060819T152718_VNIR_1.raw	Orchards and and cropped fields
2006/08/20	Magliano Campagnano		20060820T145032_SWIR_0.raw	

3.2 Data Analysis

3.2.1 Wild fire thermal analysis

The radiative transfer underlying a wild-fire observed scene is very complex: in the same area there are zones not yet touched by the fire, burning zones and zones already burnt; in the burning zones at least two distinct fire stages, flaming and smouldering, are to be considered, characterized by different temperatures, and emission rates. According to the SWIR pixel resolution, we can assume that hot pixels only include the burning zone. In this approach the firing pixel is seen as a "mesoscale" composite target made up of two "gray" bodies linearly combined through coefficients representing respectively the firing and background (no firing) pixel fraction. Of course this model is valid restricting the observation of the wild fire to the emission bands MIR and TIR.
Following Dozier et al., 1981 we assume the thermal flux for a wild fire as a function of the fractional area of two thermally distinct radiant surfaces: a surface area that corresponds to the cooler background, and the other, radiating a much higher brightness temperatures, representative of the firing portion. The model assumes that the radiative loss occurs over the whole surface of the pixel occupied by fire. We use three hyper SWIR bands to formulate a system of two equations from the simultaneous solution of the Planck equation in each band, and calculate the 'sub-pixel' temperature of the lower and hot fractions (Dozier et al., 1981; Pieri et al., 1990; Rothery et al., 1988). In this system, the three unknown quantities are represented by the temperature of the background T_b, the temperature of the hot fire Th, and the fractional area of the hottest component of the surface, fh.
Starting from these assumptions we write a system of three equations as follow:

$$\begin{cases} R_{\lambda 1} = \tau\,[fh\,(Rh_{\lambda 1}) + \varepsilon_{\lambda 1}\,(1 - fh)\,Rb_{\lambda 1}] \\ R_{\lambda 2} = \tau\,[fh\,(Rh_{\lambda 2}) + \varepsilon_{\lambda 2}\,(1 - fh)\,Rb_{\lambda 2}] \\ R_{\lambda 3} = \tau\,[fh\,(Rh_{\lambda 3}) + \varepsilon_{\lambda 3}\,(1 - fh)\,Rb_{\lambda 3}] \end{cases} \qquad (1)$$

where indices $\lambda 1$, $\lambda 2$, $\lambda 3$ are the Hyper bands used as input of the system, R is the radiance at the sensor, Rh and Rb the radiances related to the hot and background component respectively, ε is the spectral emissivity and τ the atmospheric trasmittance.
We assume three emissivity values a priori (one for each band) in order to solve the equation system. Spectral emissivity has been chosen from emissivity profiles measured in situ in post-fire locations.

Algorithm was first tested using MIVIS (multispectral infrared and visible imaging spectrometer) data acquired on active lava flow and wild fires (Fig.1). We applied an atmospheric correction using a MODTRAN model atmosphere to retrieve τ (Kneizys et al, 1983; Bogliolo et al., 1998). Herein, we take advantage of MIVIS previous data analysis to test sub-pixel algorithm on hyper imagery.

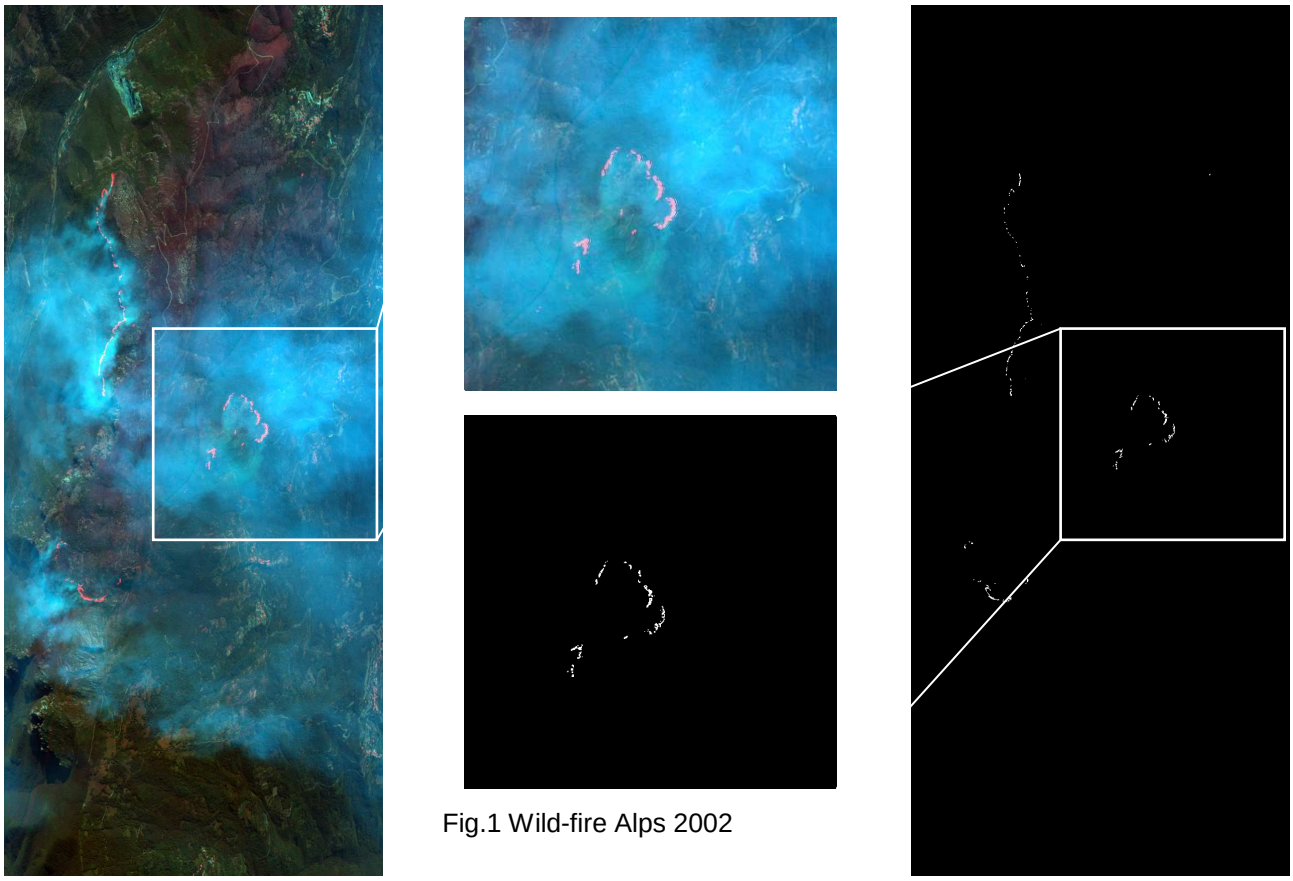

Fig.1 Wild-fire Alps 2002

Using the mathematical and physical relationships derived by the theoretical solution of the 'dual band' system equations, a new digital filter to single out lava-flows radiant pixels has been applied (Lombardo et al. 2004). This filter has been performed starting from the assumption we use the same SWIR bands (band 5 and 7, which correspond to wavelength of 2.22 and 1.65 μm respectively) of the Landsat TM in the dual band system equation (Fig.2).

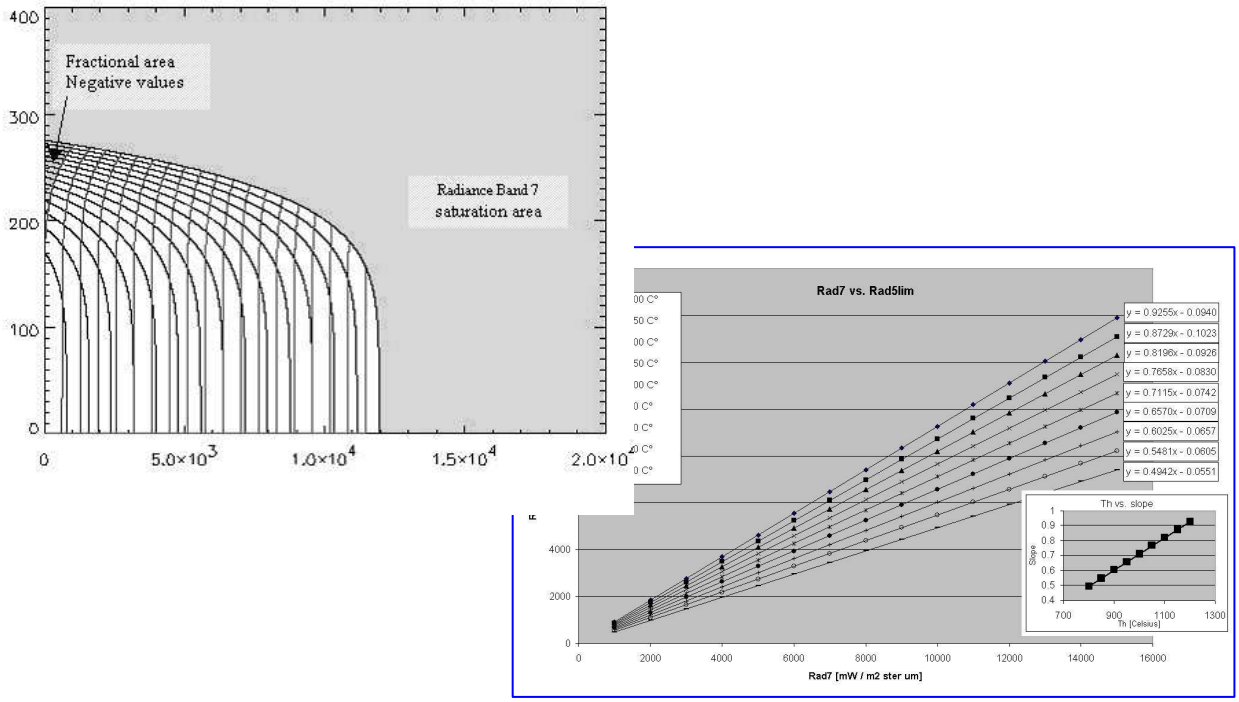

Fig.2

The plot A in Fig.3 shows the MIVIS spectral profile from a thermal pixel sample. Grey curve B is the graphic solution derived from system 1 when the lava pixel is partially filled with crusted flow at 250°C and cracks at 1000°C cover the 10% of the lava surface. A roughly comparison of the two plots highlights how MIVIS spectral profile discontinuously matches the theoretical curve B. From Fig. 2 we issue that:

- MIVIS SWIR bands are extremely noisy even after an accurate atmospheric data calibration (Lechi, 2000). This is due to a poor signal to noise ratio affecting many channels of the MIVIS SWIR II spectrometer. Band 28 and 53 (dots B1 and B2) were tested to be the most performing channels and therefore they were preferred in the solution of the dual-band equations (Lombardo et al., 2004).
- SWIR region covers only a small portion of the radiance spectrum interested by the curve B. This portion corresponds to the steep slope S_1-S_2. The dashed lines enlighten that MIVIS data lie along this slope with a broad dispersion range. This uncertainty makes difficult to solve the unconstrained system 1 by adding another SWIR band.
- On the other side, MIVIS sensor provides an excellent TIR detector. We can adjust the setting of the TIR gain in order to match our target temperature. A gain of 10 was chosen to minimize saturation effects over active lava flows. Unsaturated TIR pixels provide a reliable constraint to properly model curve B.

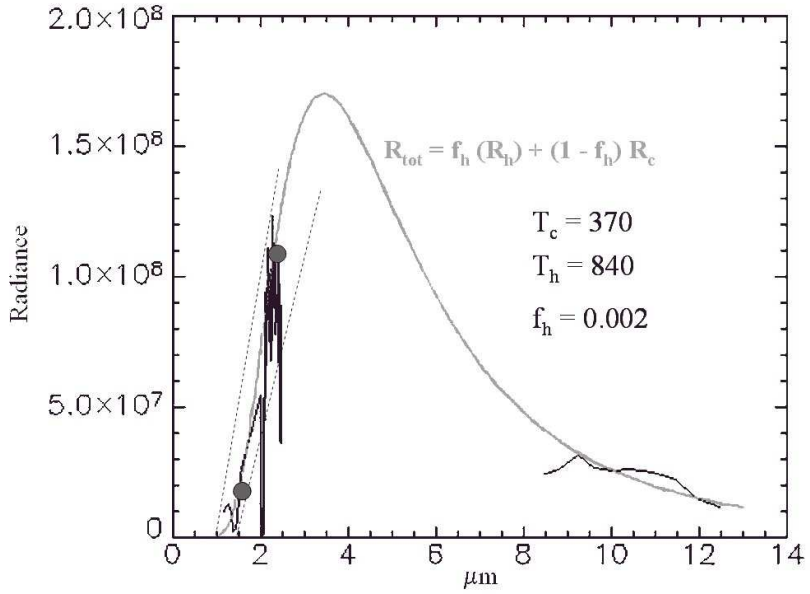

Fig.3

High radiometric resolution MIVIS data have been essential for implementing a system of three equations and solving the dual-band unconstrained system. A thermal band can greatly enhance our ability to estimate the thermal loss (Rothery et al., 1995; Oppenheimer, 1997) and the eruptive mass flux (Harris et al., 1997; Harris et al., 2000, Wright et al., 2000) both in active lava flows and wild fire.

3.3 Flame Temperature estimation using SWIR data.

3.3.1 Planck fit of the SWIR profile

In this section we describe an automatic procedure with which it is possible to extract the flame temperature with SWIR observations.

The adopted fitting method use the following assumptions:

- Because of the high resolution of the instruments (which corresponds to a scale of about 1 meter) pixels with an high flux value can be assumed to be completely covered by fire.
- The radiation emitted by the fire has a Planck spectrum:

$$I(\lambda,T) = \frac{2hc^2}{\lambda^5}\frac{1}{e^{\frac{hc}{\lambda kT}} - 1}$$

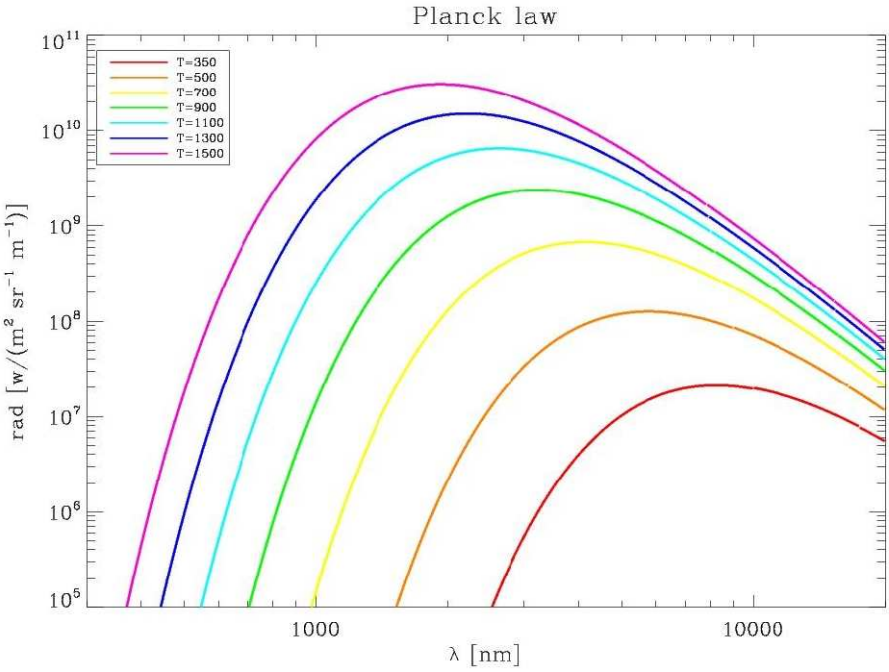

Observed spectra can contains contribution by atmospheric absorption and vegetation reflection of solar radiation. In order to study the incidence of vegetation reflected radiation in our data set we estimate the value of this quantity by a Modtran simulation and compare it to the expected emerging radiation from a fire observed with an high resolution instrument. The high resolution hypothesis is translated in the assumption that the fraction be higher then 80%. The resulting observed spectrum is then a combination of these two components. In following graphs the sun reflected radiance and transmitted are shown. The first one refers to a temperature of 800K while the second to a temperature of 1200K. It can be observed that the sun reflected component is important but much lower than the Planck emission only in the region with lambda < 1.4 micron and that this effect is relevant in the case of low temperatures.

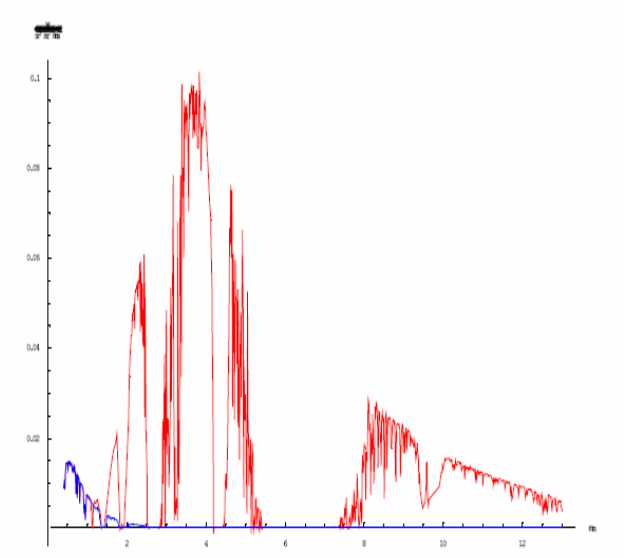

Blue line = sun reflected radiance
Red line = TOA radiance
T=800K

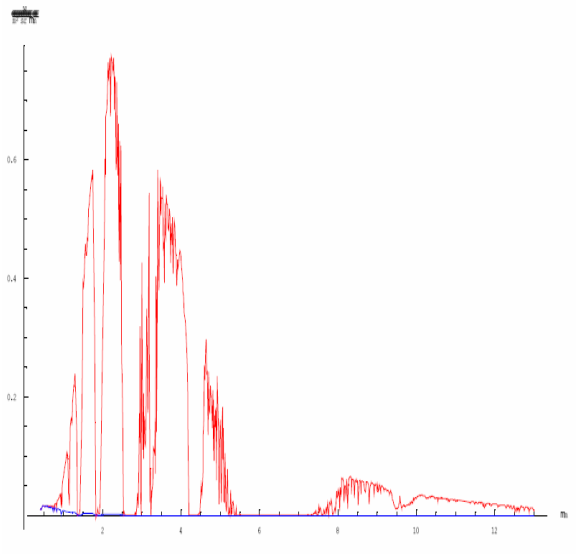

Blue line = sun reflected radiance
Red line = TOA radiance
T=1200K

This effect has been clearly observed in images collected during the campaign.
As an example we show plots of the spectra obtained in to different points: the first in the firing region the second in the background:

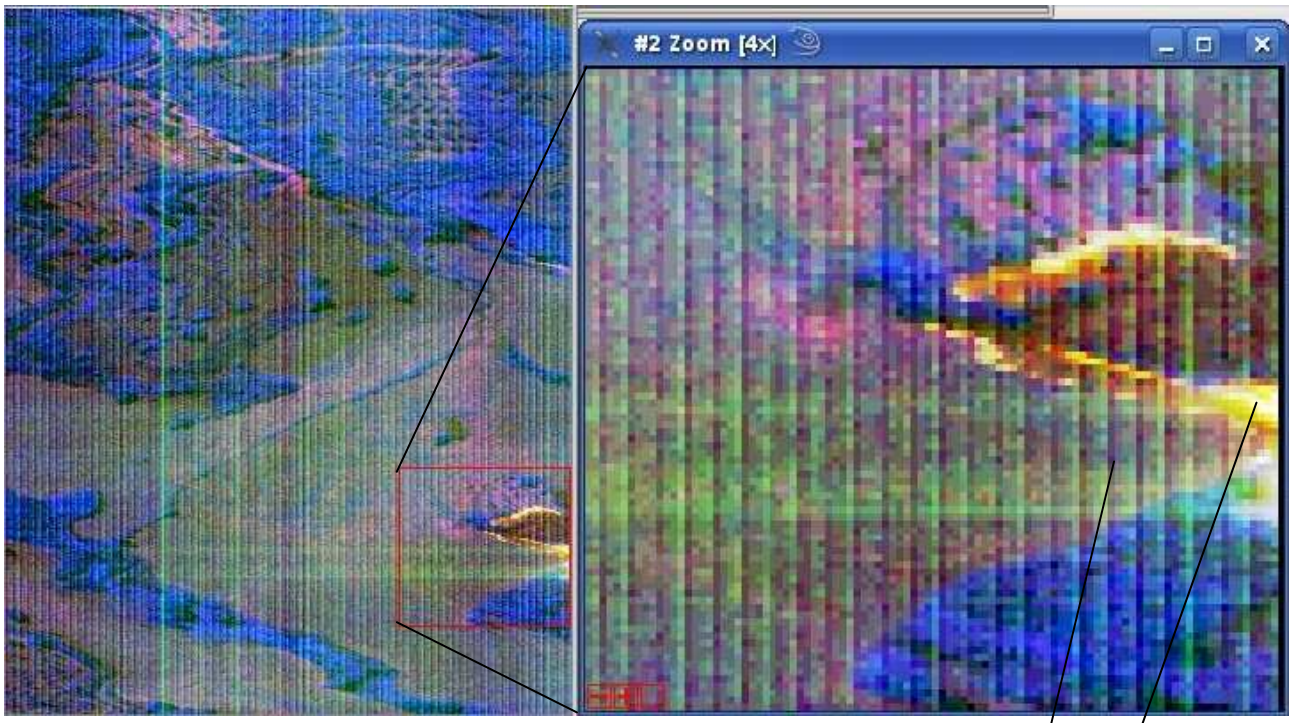

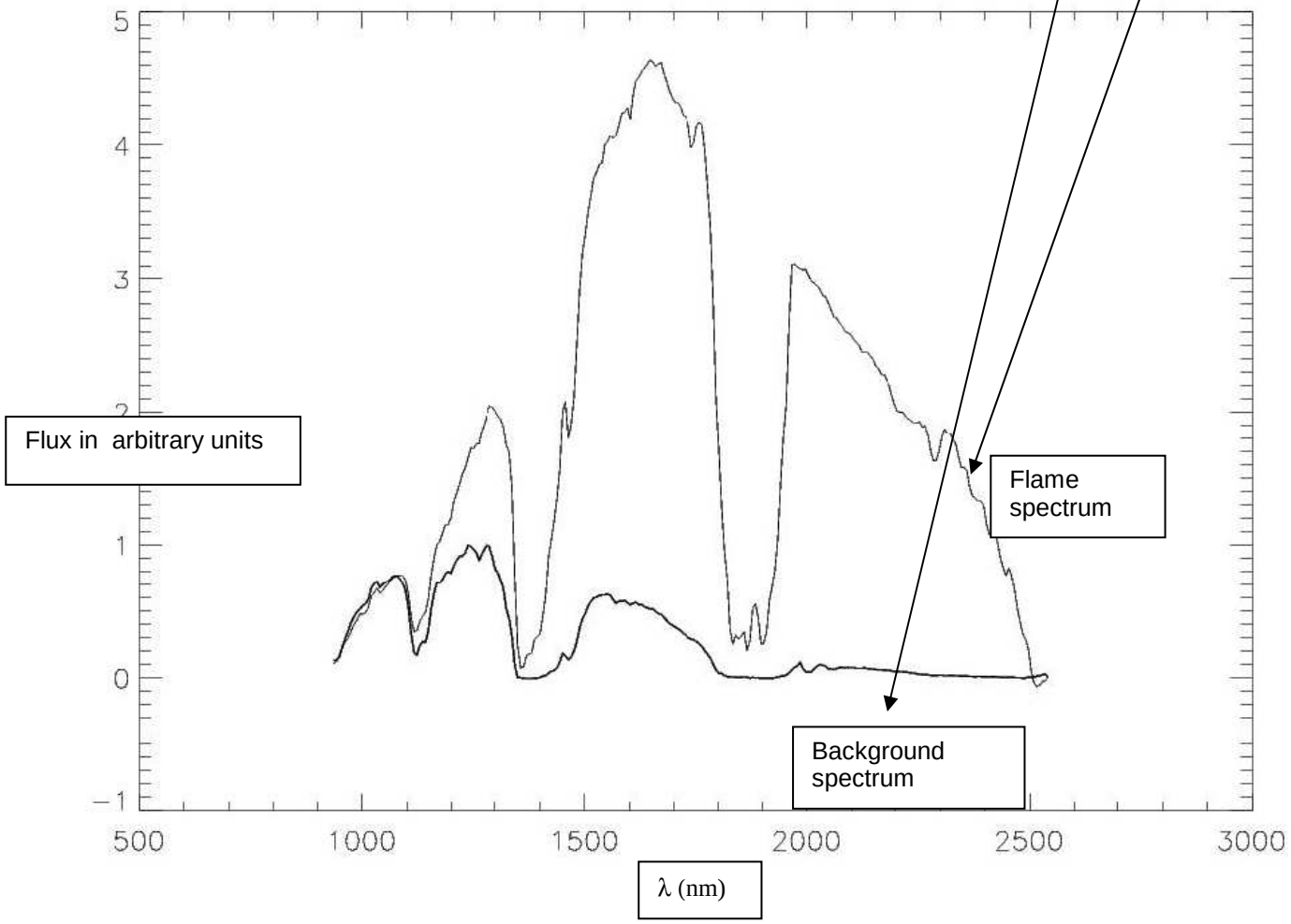

The fitting procedure avoid the region λ <1.4 nm because of the contamination with vegetation reflected radiation, and region at λ (nm) > 1.75nm where there is strong atmospheric absorption.

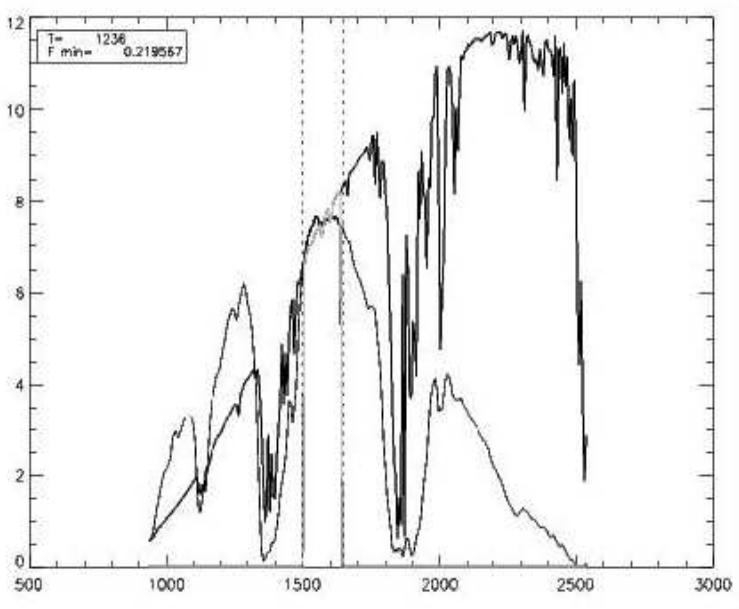

Moreover at λ > 1.65nm there is a decrease of the spectrum which seems related to some artefact of the instrumental apparatus so we choose to truncate also this part of spectrum.
In order to exclude the saturated points the algorithm firstly inspects unfluxed image and select wavelength corresponding to a flux larger then the saturation value which is 2.0^14 DN
When the remaining spectrum is too small we add a VNIR region in particular wavelength from (1.2,1.3). This seems reasonable because below strong fires we don't expect significative emission by vegetation.

An example of the remaining window is shown in the figure above corresponding to the two shaded lines in the case of no saturation effect. The non linear last square fit procedure restricted to the region discussed above has been realized and tested over a simulated dataset where the simulated spectra have been realized by a convolution with a Planck function and a standard atmospheric model.

3.3.2 Temperature fit using Galileo calibrated images

We tried to adapt the "sub-pixel temperature" algorithm to Hyper data by using SWIR data calibrated and processed by Galileo. Unfortunately, three-bands technique (Eq.1) frequently fails when applied on hyper data. Data calibrated by Galileo show brightness temperatures of 400-500°C for hot-pixels. These values are extremely low when compared with temperatures of 900-1000°C expected for 1 m^2 pixel completely filled with burning vegetation. Some further investigations on the data calibration may improve the quality of results.
Different approach has been used to validate these assumptions:

– We use a gradient-expansion algorithm to compute a non-linear least squares fit to a user-supplied function

  Rtot = fh (Rh) + el (1 - fh) Rb

  with 3 parameters.

  fh , Th , Tb

– The user-supplied function is the two thermal components equation where the partial derivatives are known
– Spectral emissivity values of background were provided by ground measurements retrieved using the FieldSpec Pro field spectrometer.

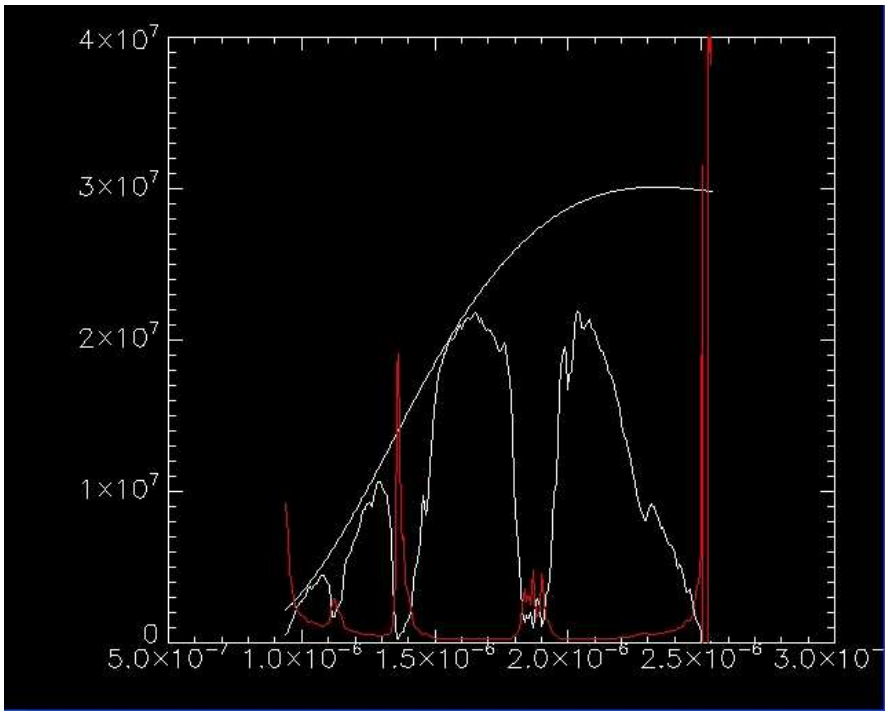

Fig.4

Figure 4 shows the result of non-linear least squares fit for a fire sample pixel. The white spectrum is the original hyper signal. Red plot represent intensity of atmospheric absorption. Wavelengths affected by strong atmospheric absorption have been excluded in temperature computation.

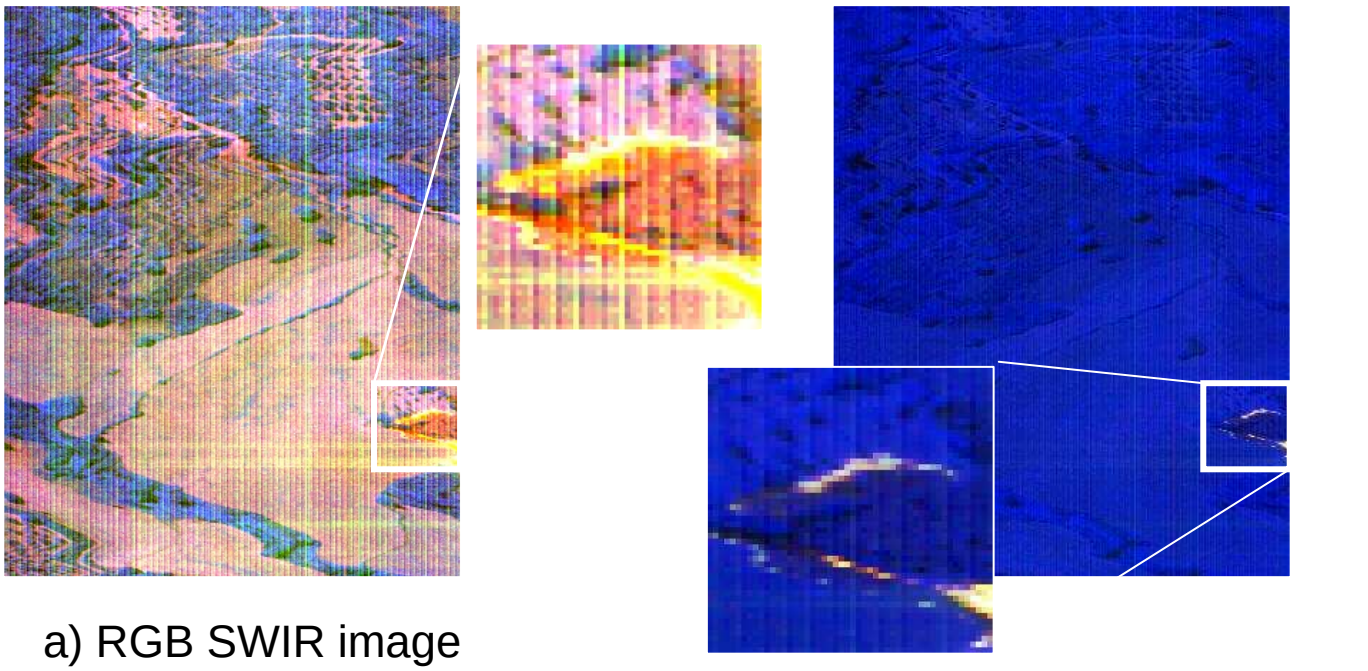

a) RGB SWIR image

b) Hot temperature distribution

Fig.5

Figure 5b shows the temperature map of wild fire developed on 04th august 2006. Sub-pixel solutions are characterized

by very low and unphysical value of the hot fraction (0.0001-0.001) and very high fire temperatures (1000-1300°C). These results have to be discarded because a so small fraction is unphysical and not in good agreement with field observations. We expect higher value of fractional area for pixels entirely filled with burning vegetation, considering the special resolution of hyper data (about 1 m^2). On the other hand, fire temperatures appear to be anomalously elevated with respect experimental measurements of 900-1000°C.

3.3.3 normalization

A first attempt has been made to normalize flux spectra for an arbitrary band:

$$F(\lambda)' = F(\lambda)/F(\lambda_0)$$

This operation is undependent of uncertainties in the flux calibration but brings sometimes to very high temperatures which seem incorrect. This is probably an effect of the adopted normalization which constrain the solution only with to the shape of the spectrum which is in addition contaminated by the instrumental effect of the strong decrease after 1650 nm.

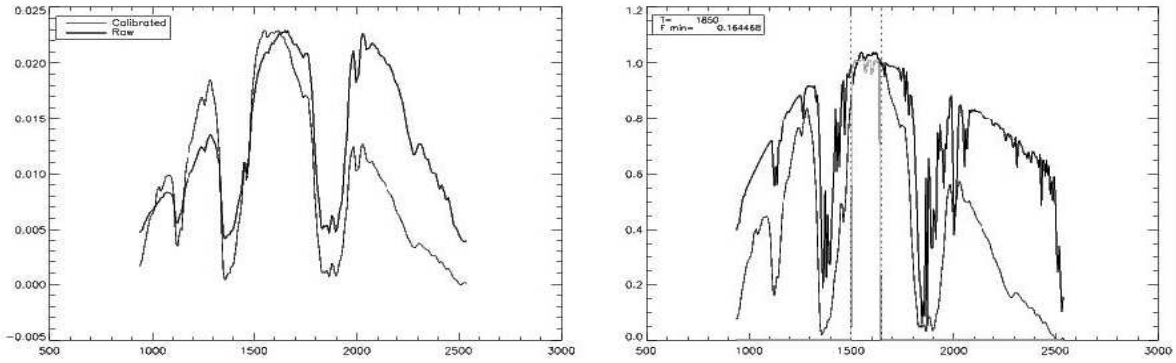

3.3.4 Planck normalization

The second and adopted solution consist in a numerical comparison between the calibrated with unknown scale factor image and the Planck function which we expect to represent the emission emerging from radiant pixels. Numerically we have:

$$Planck\ (T = 1400\ K, \lambda = 1500\ nm) = 16.6[W/m^2 sr \cdot m]$$

One of the most intense pixel in the 04/08/2006 image has as:

$$\text{HYPER}(04/08/2006,\ \lambda = 1500 nm) = 0.05$$

We impose for this image an adimensional scale factor of 300. After the application of this scale factor to the images we apply the algorithm of temperature fitting obtaining results shown in the following figures:

3.3.5 maps

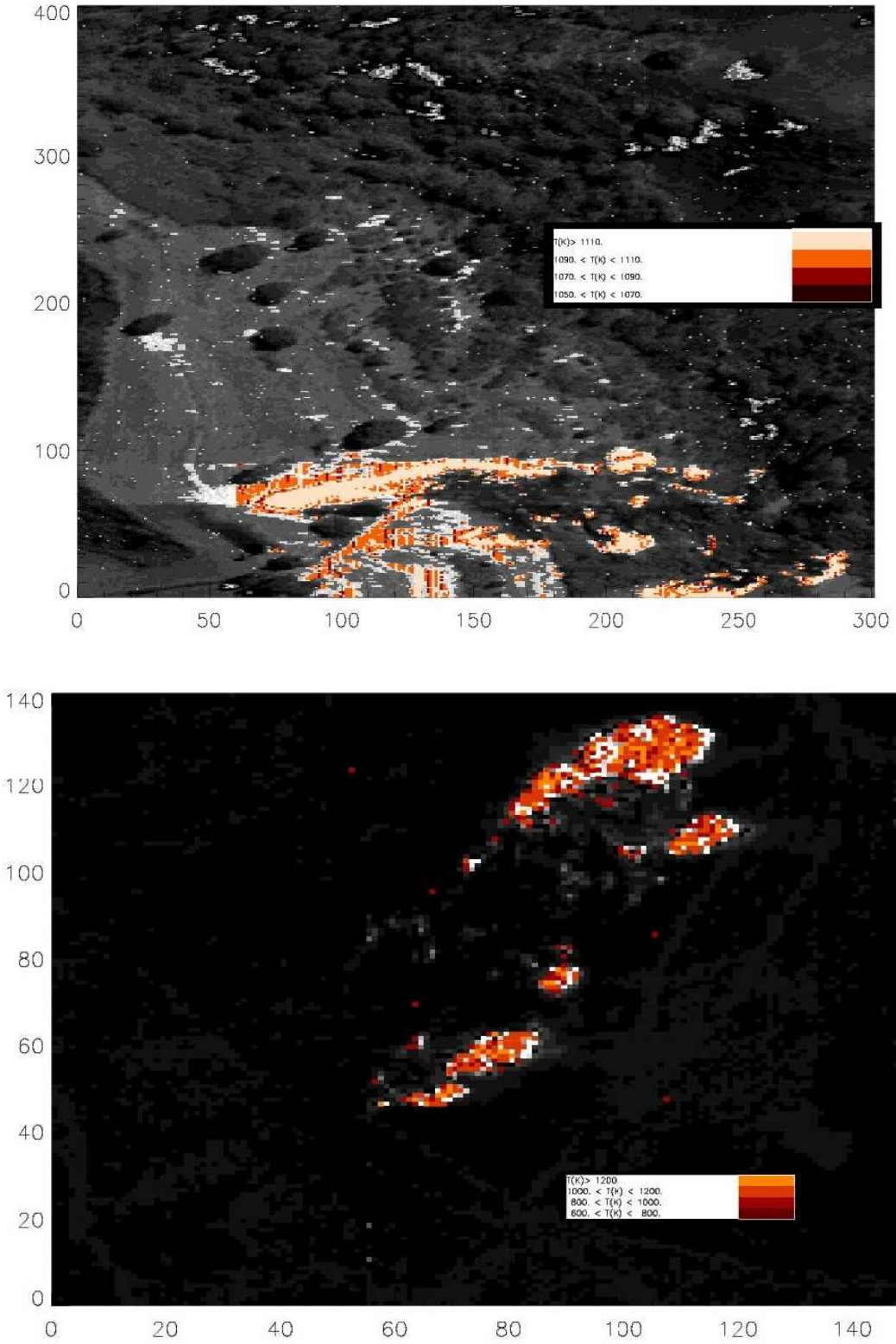

Figure 6: Map of 14/08/2006 computed with the images rescaled by the arbitrary calibration factor.

3.4 Fire map using K line method

3.5 K line analysis

The HYPER high spectral resolution allows to apply different methods for wild fire analysis. Firstly we check and verified Vodacek (Vodacek et al., 2002) theory . The study was devoted to investigate improvement due to the good spectral performances of HYPER sensor.
Because K emission is specific to flaming combustion of biomass, it is potentially possible to detect flaming area. According Vodacek study, the scene at 589 nm point out smoke from fire while the 770 nm image shows a good penetration from smoke
We apply this and show the results on August 14 2006 data acquired on Oriolo village area. We choose this data set because of low image spatial distorsion.

Figure A) and B) show the scene at 589 and 770 nm.

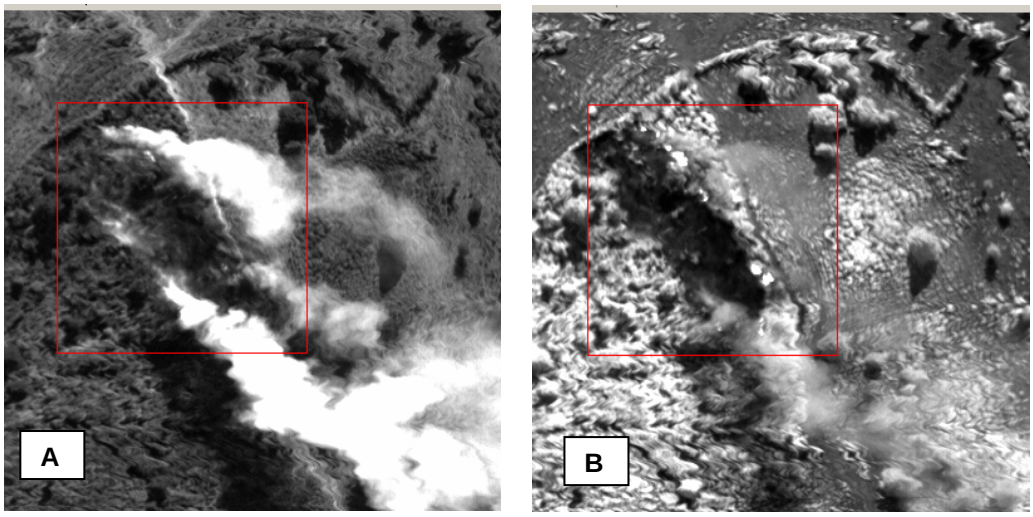

Figure August 14 2006 on Oriolo A) 589 nm and B) 770 nm image.

The band 770 is in correspondence of K emission peak and was used by Vodacek because of spectral resolution of AVIRIS (9 nm). Due to the very high HYPER spectral resolution it is possible to show the images at 766.5 and 769.3 (HYPER bands) almost in correspondence of K lines (766.5 nm and 769.9 nm) really corresponding to flaming area (Fig A and B)

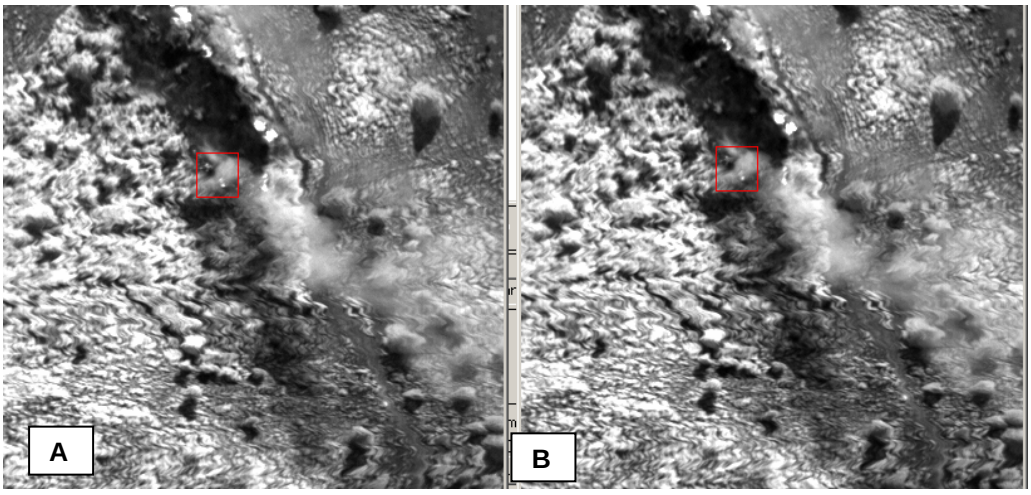

Figure August 14 2006 on Oriolo A) 766.5nm and B) 769.3 nm image.

If we plot the spectral profile we can see the K douplet in the flaming area not covered by the smoke (A) and with an attenuated value also under the smoke (B).

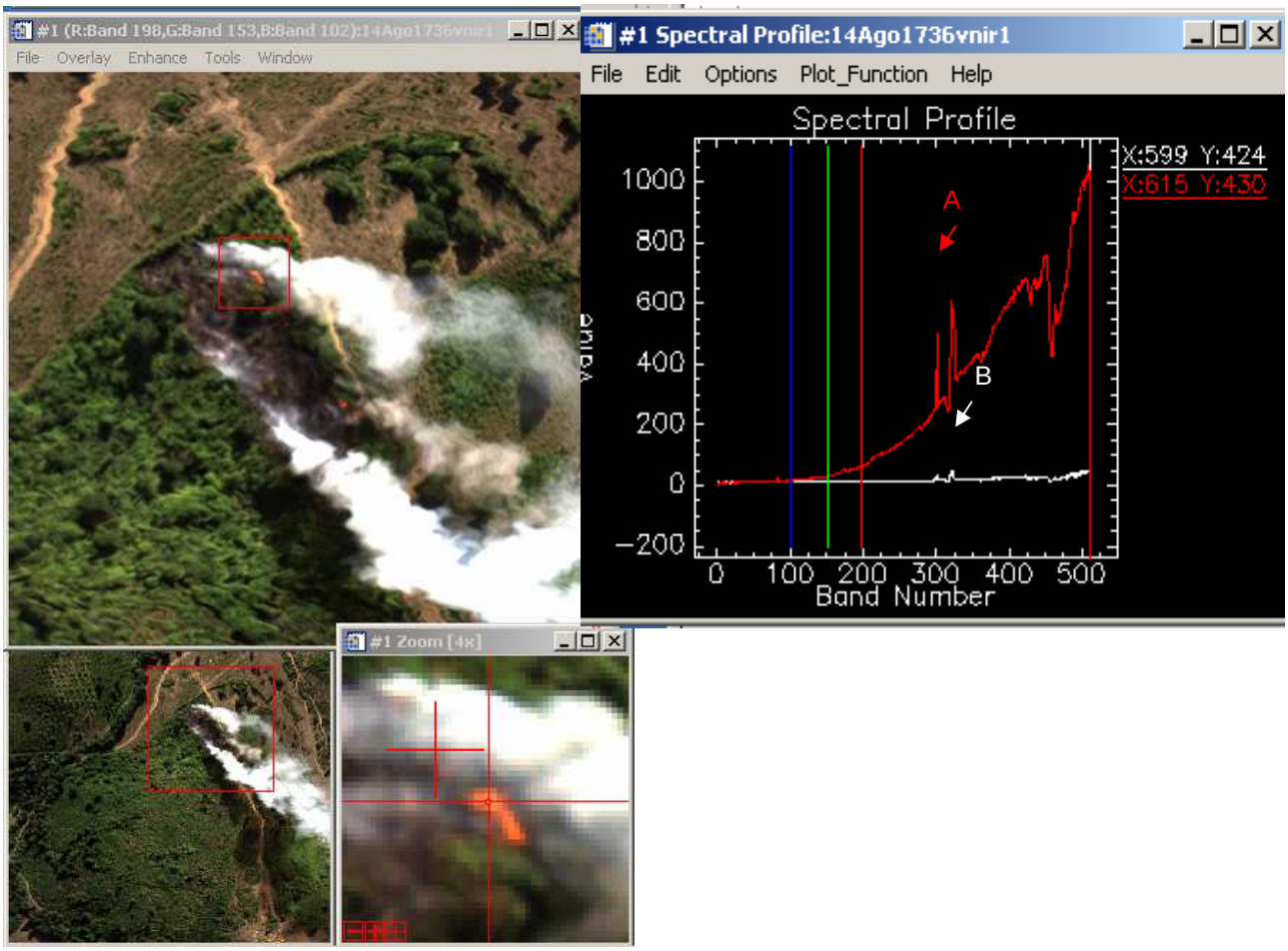

Figure K doublet detected in correspondence of flaming. Smoke attenuates the signal allowing to K pick visible also in the case of smoke covered pixel

Band ratio analysis

Rationing is an enhancement process in which the DN value of one band is divided by that of any other band in the sensor array.
Certain ratios can point to certain tonal anomalies that are diagnostic of special conditions. We applied the band ratio In order to point out the fire active sources.
The bands ratio (766.3nm/779.0 nm) was applied on August 14 image. Gaussian Enhancement was applied. The ratio points out tonal anomalies in correspondence of K emission and result to be diagnostic of flaming area.

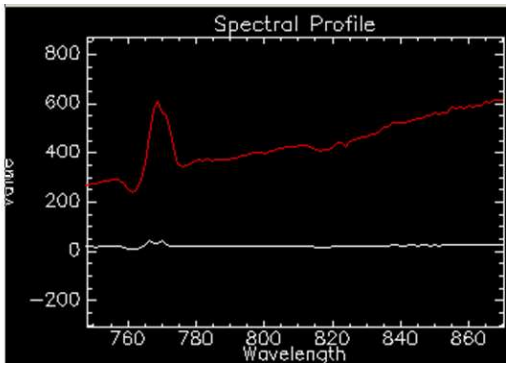

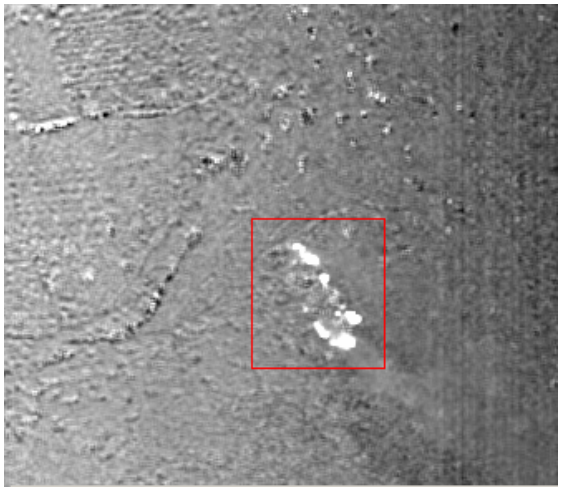

Figure The bands ratio (766.3nm/779.0 nm) on August 14 2007 image.

No information is provided regarding the front of fire or smouldering area that are not interested by K emission.

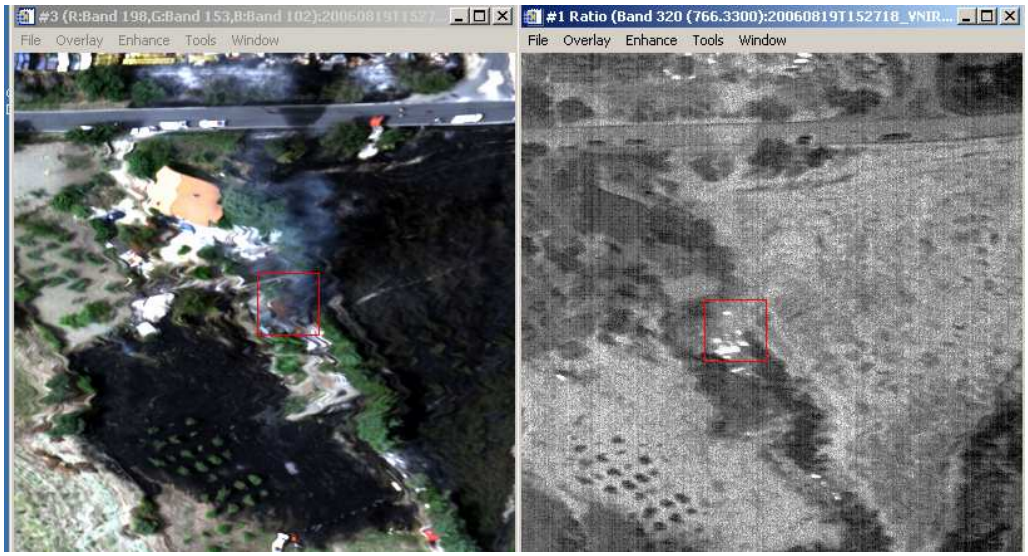

The bands ratio (766.3nm/779.0 nm) on August 19 2007image.

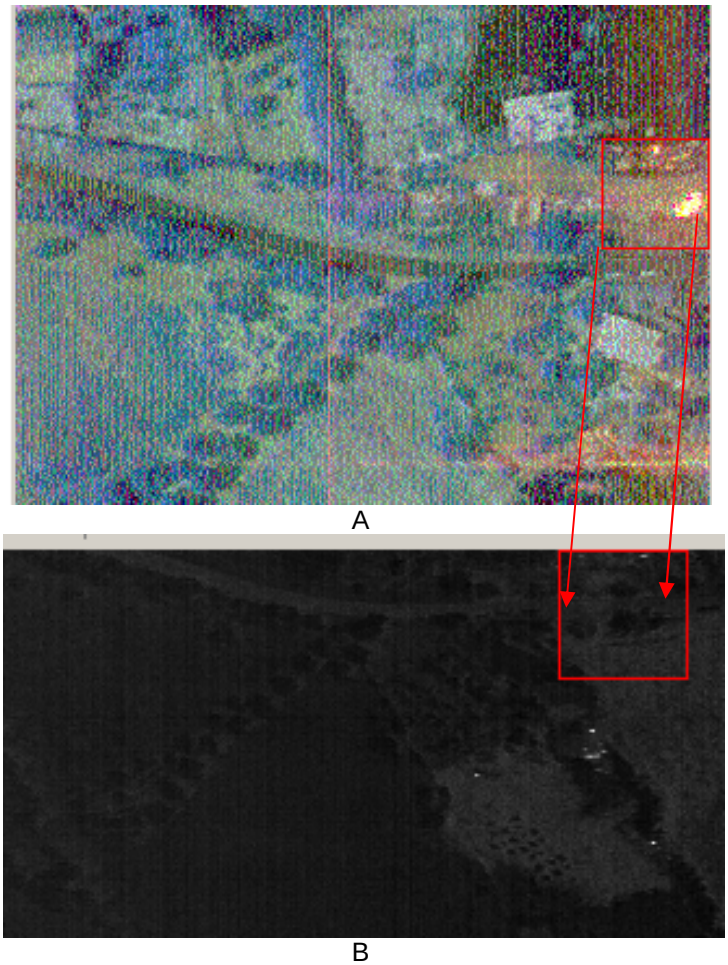

A

B

August 19 2006 15:27 SWIR (A) and Resized VNIR (B) band ratio image.

The bands ratio (766.3nm/779.0 nm) on August 16 2006 image.

3.5.1 HYPER SWIR –VNIR comparison.

SWIR range is best for fire scientific analysis from different point of view: firstly because of large difference between fire and background, secondly because of the minimal clutter in emissive spectra.
In order to point out potentiality and limits of K emission analysis a comparison was performed. The image data in the Visible range acquired on 14 August 2006 was spatially resampled to be comparable with the SWIR one, acquired at the same time.
The bands ratio (766.3nm/779.0 nm) has been compared with the SWIR image (R=38, G=75, B=58).
A spatial filtering operation was performed to suppress the random noise.

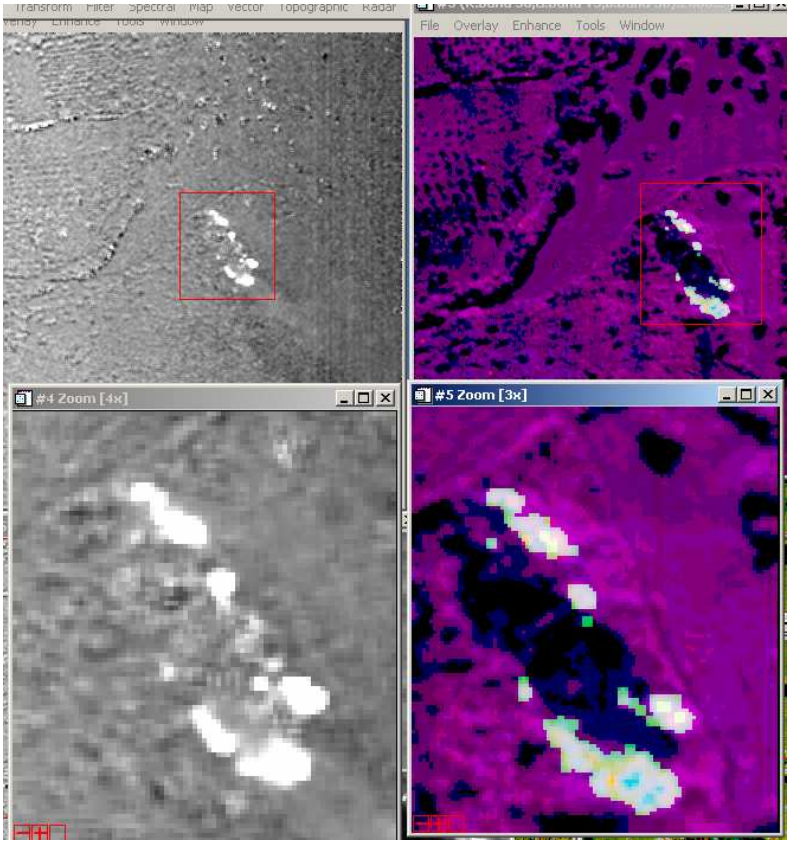

4 Satellite and airborne data comparison

4.1 satellite data selection

Remotely-sensed data: used in the spectral analysis

Low spatial resolution data was acquired by the AVHRR antenna INGV.
High spectral-spatial resolution satellite data was a wild fire acquisition in the same period of Italian flights.

Satellite	Target	Date	Comments
AVHRR	Central Italy	August 14th 2006 (15:33) August 4, 9 19, 2006	Lat 2° 08' 26.873" nord Lon 12° 25' 03.288" West No good weather condition o resiolution insufficient compared to fire extention

HYPERION	Northeast of Tucson, Arizona	July 12, 2003.	Lat: 32.427 North Lon 110.768 West. 84,000 acres and destroyed 333 structures
MODIS	August 5 e 13 2006		No evidence for fires
SEVIRI		Whole period with a frequency of 15 min	No evidence for fires

4.1.1 NOAA-AVHRR station, INGV

NOAA-AVHRR station, which is made of a fully integrated antenna tracking and ground station for receipt of Advanced Very High Resolution Radiometer (AVHRR) satellite imagery and comprehensive software systems for AVHRR image processing and data analysis.
The INGV antenna has a diameter of 0.46 m that allows a full coverage of the mediterranean region (smaller circle).

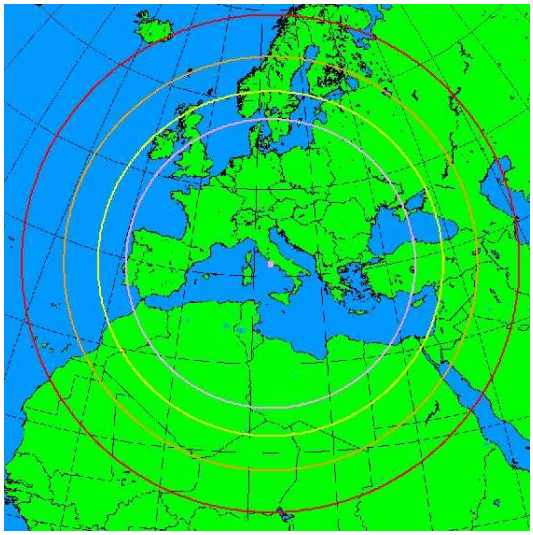

During the AIRFIRE project it was possible to detect by AVHRR the two largest fires occurred in Oriolo area as we show in the following two images

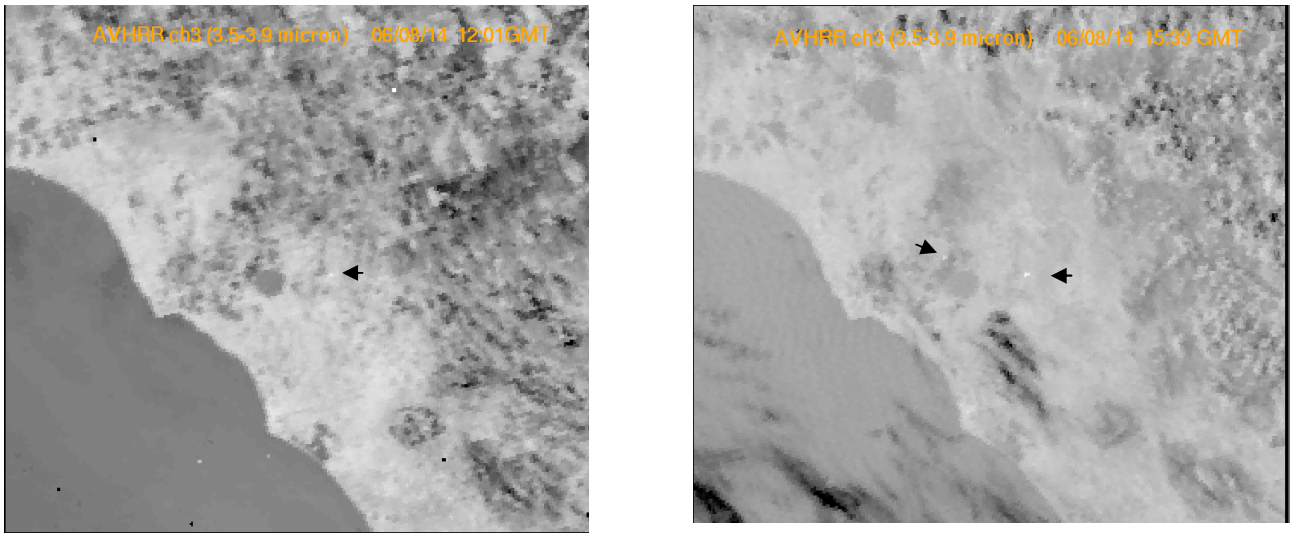

Fig a AVHRR Middle Infrared band(3.5-3.9 micron) detect the first and second fire in Oriolo area.

The Brightness temperature of the warm pixel in the 3.5-3.9 micron band is 45< =Tb>50C.

4.1.2 MODIS

Modis data avalaible are summarized in the table above. Due to the short duration of fire compared to the revisiting time of MODIS no fire was acquired by this sensor.

4.1.3 Hyperion data

Hyperion is an hyperspectral sensor on board of the Earth Observing-1 (EO-1) satellite. Hyperion collects 220 unique spectral channels from 0.357 to 2.576 micrometers with a 10-nm bandwidth and a spatial resolution of 30 meters). http://eo1.gsfc.nasa.gov/overview/eo1Overview.html
The selected data referrers to Aspen fire; it was located immediately NE of Tucson, Arizona, and started on June 17, 2003. The fire burned over 84,000 acres and destroyed 333 structures
The Hyperion data was analyzed to compare different scale data and different spectral, spatial features with HYPER data.

The following picture shows a calibrated radiance spectrum of thee Hyperion in calibrated data of Hyperion in correspondence of a burning zone for VIS-IR range.

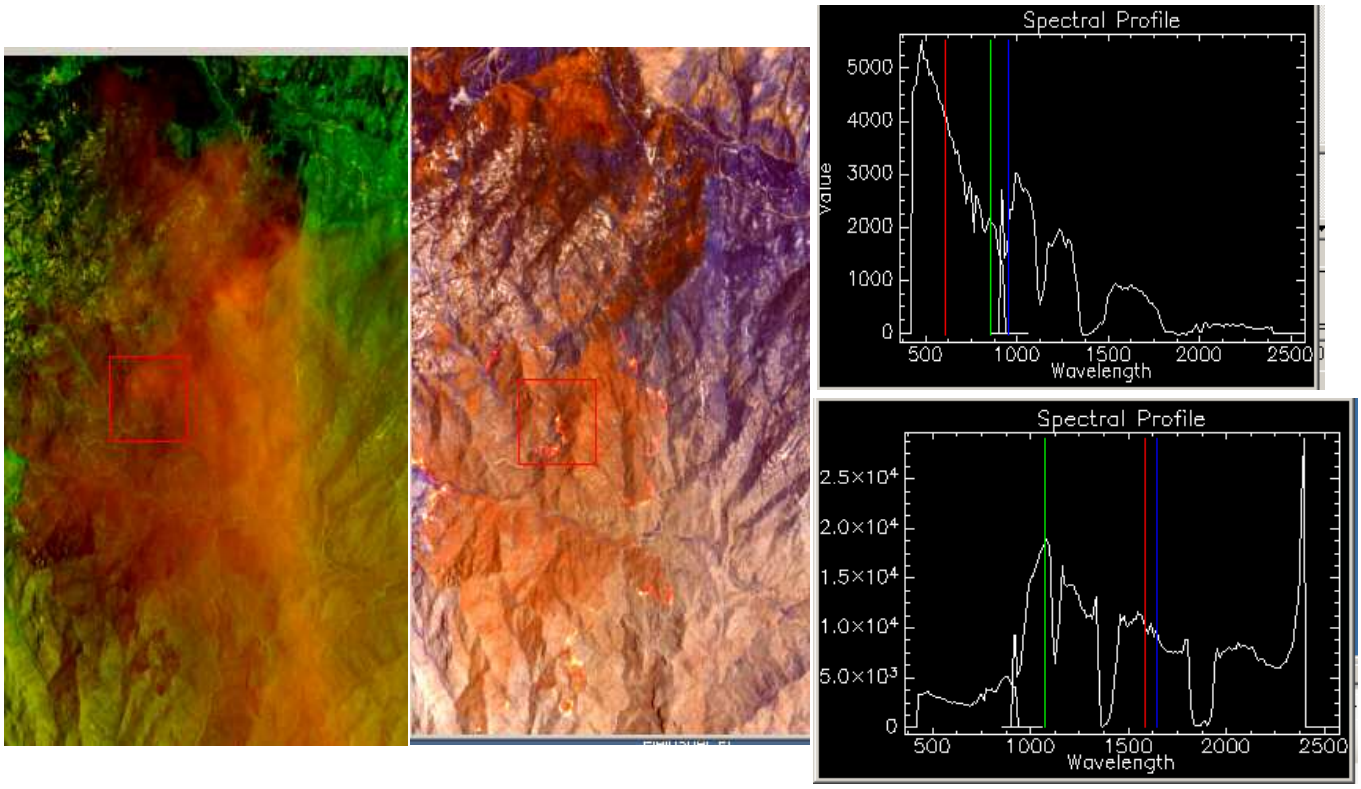

The fig. shows a zoom of the burning area in R=609nm G=854.1nm and B= 955.5nm.
A and in R=2224nm, G=1568nm B=1245 nm B. The plotted spectra are referred to a radiance spectrum in the smoked area (Up) and hottest pixel (down)

The SWIR range of Hyperion shows the flaming area and the front of fire also under the smoke. If we want to use the radiance warm pixel spectra we find again the AVHRR saturation problem.

4.2 Satellite data analysis

Before examining real data, a sensitivity analysis has been performed in order to study the fire visibility intended as the minimal fire size necessary for detection with the two sensors of interest (AVHRR and SEVIRI). The MIR channel has been considered due to its greater sensibility to this phenomenon.
It has been assumed that it is possible to issue that a pixel is interested from fire when its radiance is strongly greater than the fluctuations due to instrumental characteristics.
In order to give numerical estimations, an homogeneous area (surrounding the region of interest) has been considered on both AVHRR and SEVIRI images: in this area the measured radiance standard deviation has been retrieved and the fire presence condition has been formalized as follows:

$$L_{fire} > L_{background} + 3\sigma$$

This equation gave a minimum radiance for the two sensors, that, a given temperature, corresponds to a minimum pixel fraction that, in turn, gives the minimum detectable fire dimension with respect to weather condition and observing condition.
The results for three reasonable temperature (800K, 1000K, 1200K) are reported below in figure and table, we compute the average and standard deviation for images of 14/08/2006, the σ value can change for different days.

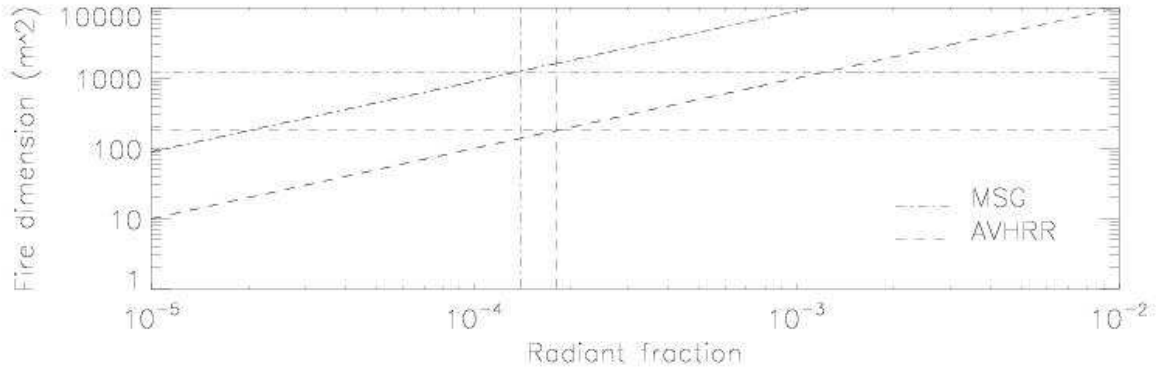
Fire dimension (m^2)
10000
1000
100
10
1
10^{-5}
10^{-4}
10^{-3}
10^{-2}
Radiant fraction
MSG
AVHRR

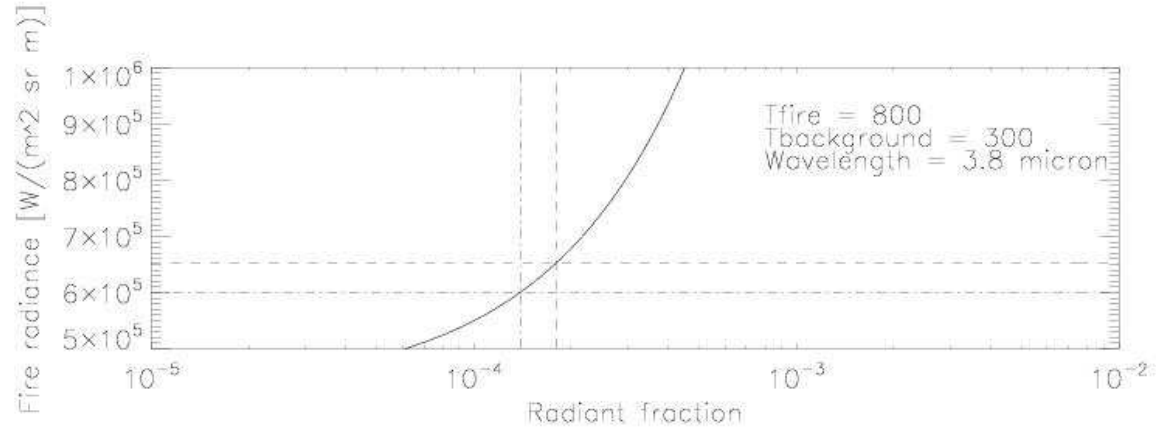
Fire radiance [W/(m^2 sr m)]
1×10^{6}
9×10^{5}
8×10^{5}
7×10^{5}
6×10^{5}
5×10^{5}
10^{-5}
10^{-4}
10^{-3}
10^{-2}
Radiant fraction
Tfire = 800
Tbackground = 300
Wavelength = 3.8 micron

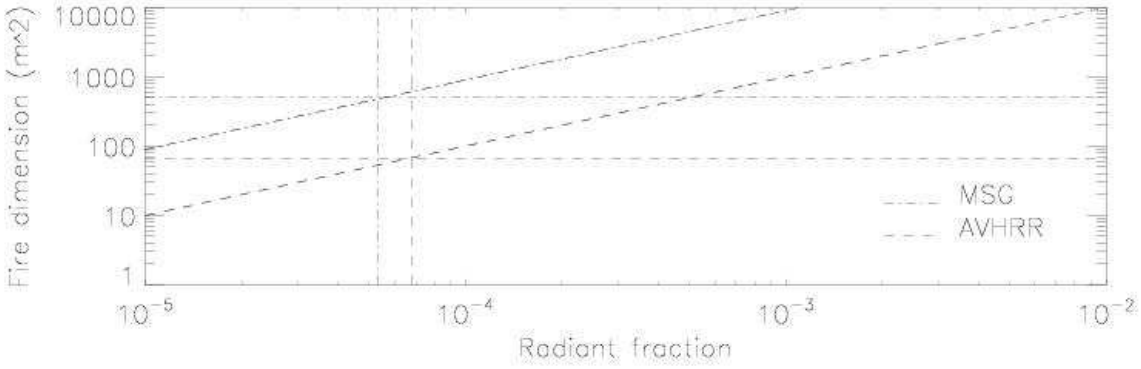
Fire dimension (m^2)
10000
1000
100
10
1
10^{-5}
10^{-4}
10^{-3}
10^{-2}
Radiant fraction
MSG
AVHRR

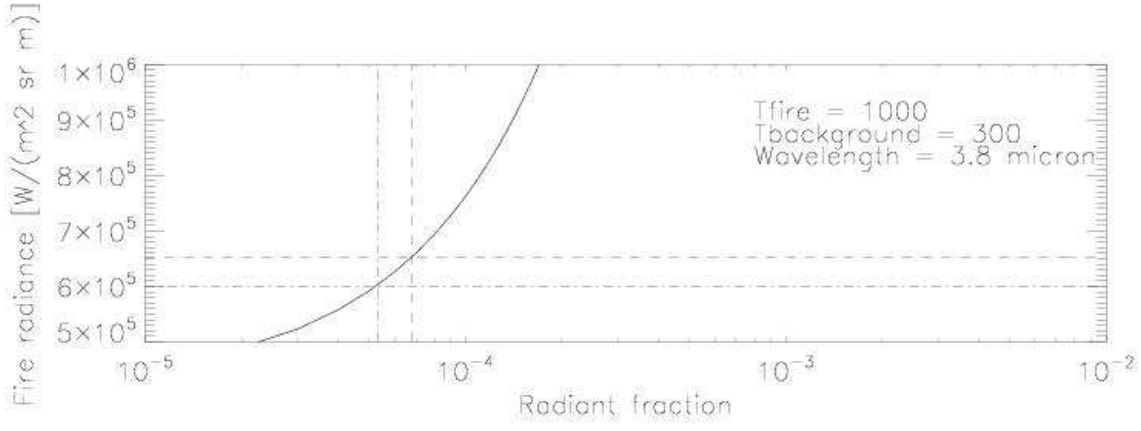
Fire radiance [W/(m^2 sr m)]
1×10^{6}
9×10^{5}
8×10^{5}
7×10^{5}
6×10^{5}
5×10^{5}
10^{-5}
10^{-4}
10^{-3}
10^{-2}
Radiant fraction
Tfire = 1000
Tbackground = 300
Wavelength = 3.8 micron

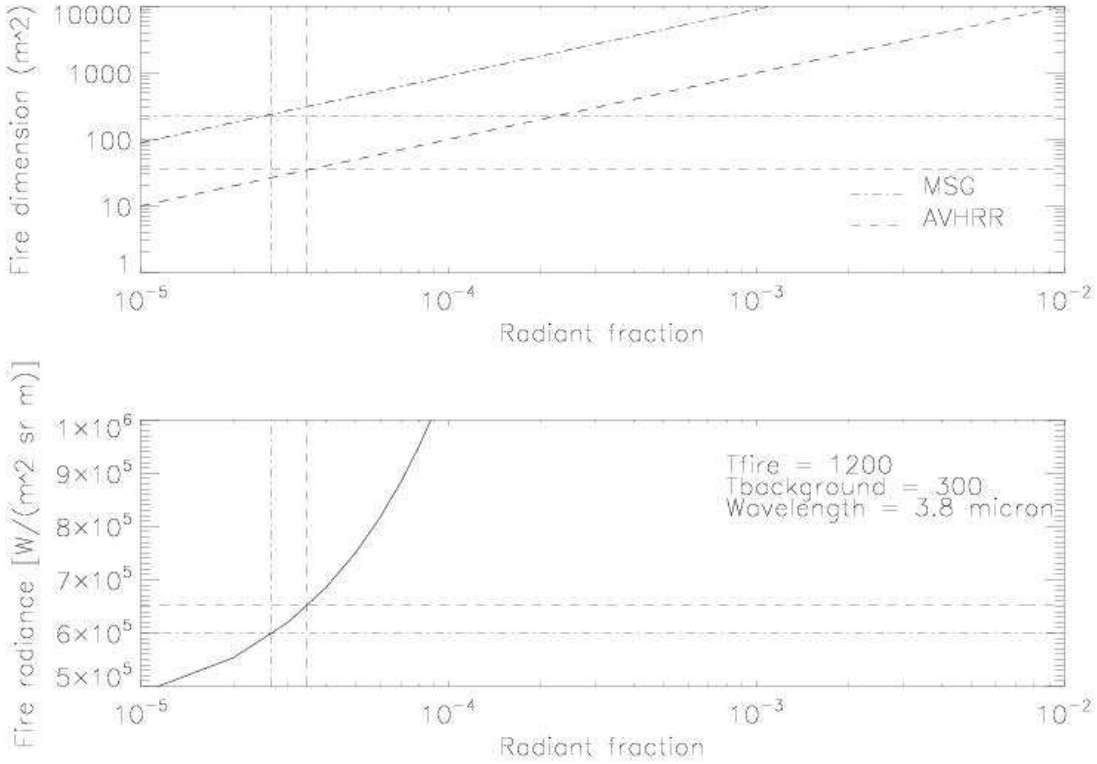

		T = 800 K	T = 1000 K	T = 1200
AVHRR	Minimum fractional area	$1.9 * 10^{-4}$	$6.8 * 10^{-5}$	$3.45 * 10^{-5}$
	Minimum fire dimension	180 m^2	65 m^2	35 m^2
SEVIRI	Minimum fractional area	$1.5*10^{-4}$	$5.3*10^{-5}$	$2.65*10^{-5}$
	Minimum fire dimension	1200 m^2	500 m^2	230 m^2

Figure 4-1: minimum size of detectable fires for 14/08/2006 images

4.2.1 AVHRR

At first AVHRR was approached because of its better spatial resolution (1 km x 1 km). Two images were taken into account, one at 12.01 UTC and the other at 15.33 UTC. A visual inspection on the MIR channel in 15.33 image confirmed the presence of pixels that could contain fires. As it can be seen in the below figure, the geographical location corresponds to the areas of Oriolo and Magliano/Campagnano, where plane flew collecting measures.
Also in 12.01 image there's a pixel in Magliano/Campagnano area candidate to be a burning area.

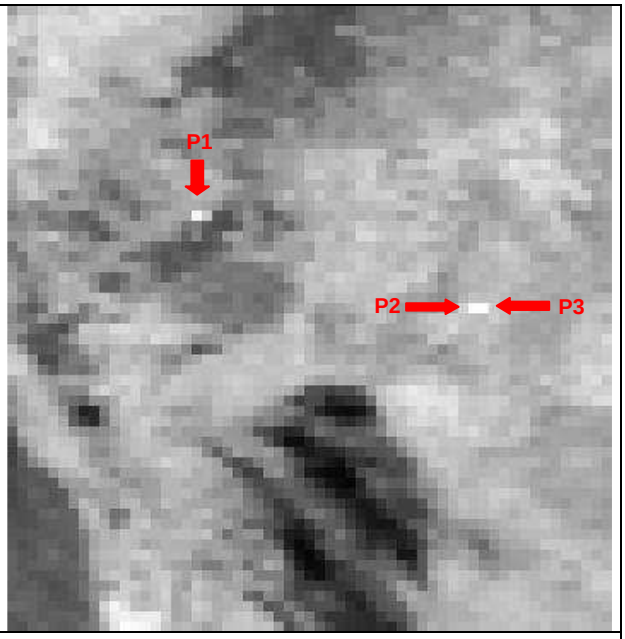

15.33

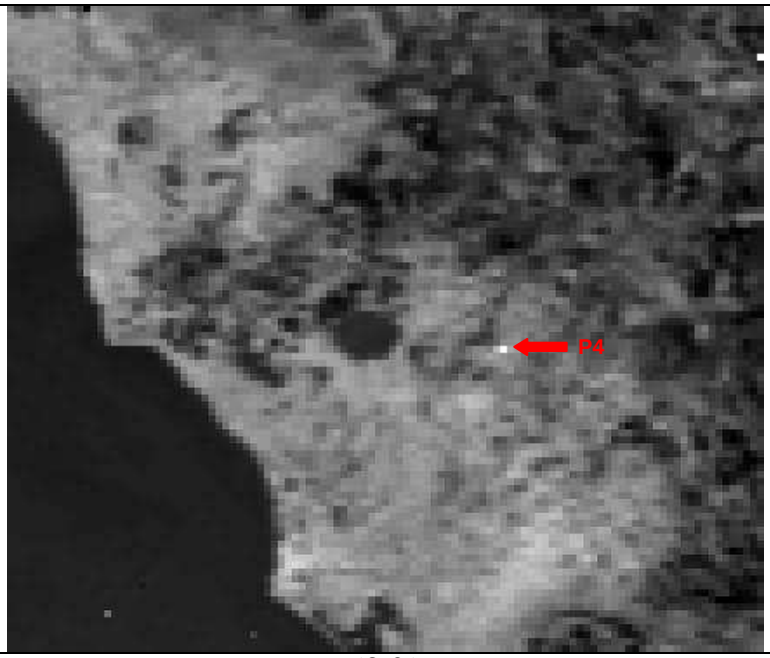

12.01

Statistics computed in a restricted area of the two images confirmed the presence of four pixels over the statistical fluctuations. Values are reported in tables below:

Image	Minimum	Maximum	Mean	Standard Deviation
12.01	350310	1229660	672023	135830
15.33	171580	1022330	469700	72200

	Pixel value	Distance from the mean
P1	672020	~3 St.Dev.
P2	1022330	~8 St.Dev.
P3	836450	~5 St.Dev.
P4	1229660	~4 St.Dev.

Once identified the pixels of interest, data have been processed; a minimization method has been adopted to minimize

the difference between the measured radiances and the expected values computed with function *F*, described below:

$$F = fP(\lambda, T_1) + (1 - f)P(\lambda, T_2)$$

where
f = radiant fraction in the pixel
T_f = fire temperature
T_b = background temperature
P(λ,T) = Planck function

Several trials have been carried out and it has been noted that there was a strong connection between the results and the starting point for the minimization procedure. This consideration led to introduce a preliminary step in order to choose a suitable starting point: the model has been computed on a grid of values obtained varying each parameter between maximum and minimum expected values and the set of parameters corresponding to the point closest to measures has been elected as starting point.

Fit results are reported below.

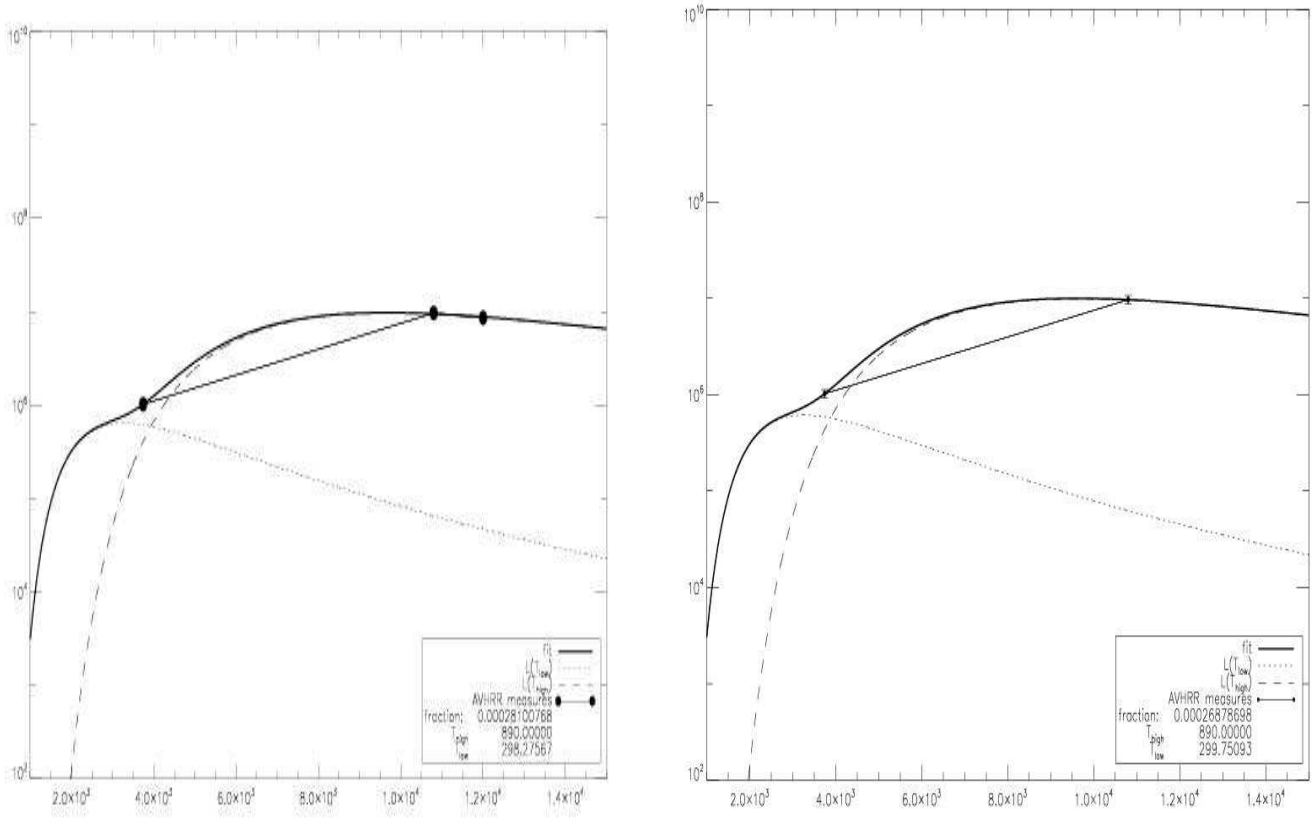

The figures shows fit result of the function computed as the sum of a Planck function with low temperature and a Planck function with high temperature.

It is worthwhile noticed that if, for the same fit, only one TIR channel is used, results don't change meaningfully; figures reports the results for the pixel P2 and table compares results in the two fit processes.

	Fit 2 TIR	**Fit 1 TIR**
T_f	890	890
T_b	298	299
Radiant fraction	0.00028	0.00026

Further considerations about channels and fitting will be carried out in next Section. A quick look to results in this pixel (which is the strongest among the three ones in exam) has put on alert because of the very low fire temperature retrieved, suspiciously close to the lower bound imposed in fire temperature computation.
Therefore, the function to be minimized in the retrieving process has been further analyzed and it has been discovered that it has no real minimum, so, the lower bounds are imposed the lower results come out for temperature.
Then measures have been interpreted using the same procedure used to identify the starting point with the conditions that:

- the expected values must be greater than the measures, which are affected from atmospheric attenuation;
- the difference between model and measures must be within 10%.

Results obtained through this constrained minimum method are reported in table below:

Pixel of interest	Fire temperature	Background temperature	Radiant fraction
15.33-P1	950	300	0.0001
15.33-P2	980	300	0.0002
15.33-P3	950	300	0.00015
12.01-P4	950	310	0.0002

4.2.2 MSG

In MSG case, too, a preliminary visual inspection on SWIR and MIR channels has been performed. The greater amount of data available makes possible to look at the scene evolution in correspondence to the airplane flight time (and more), which is displayed here:

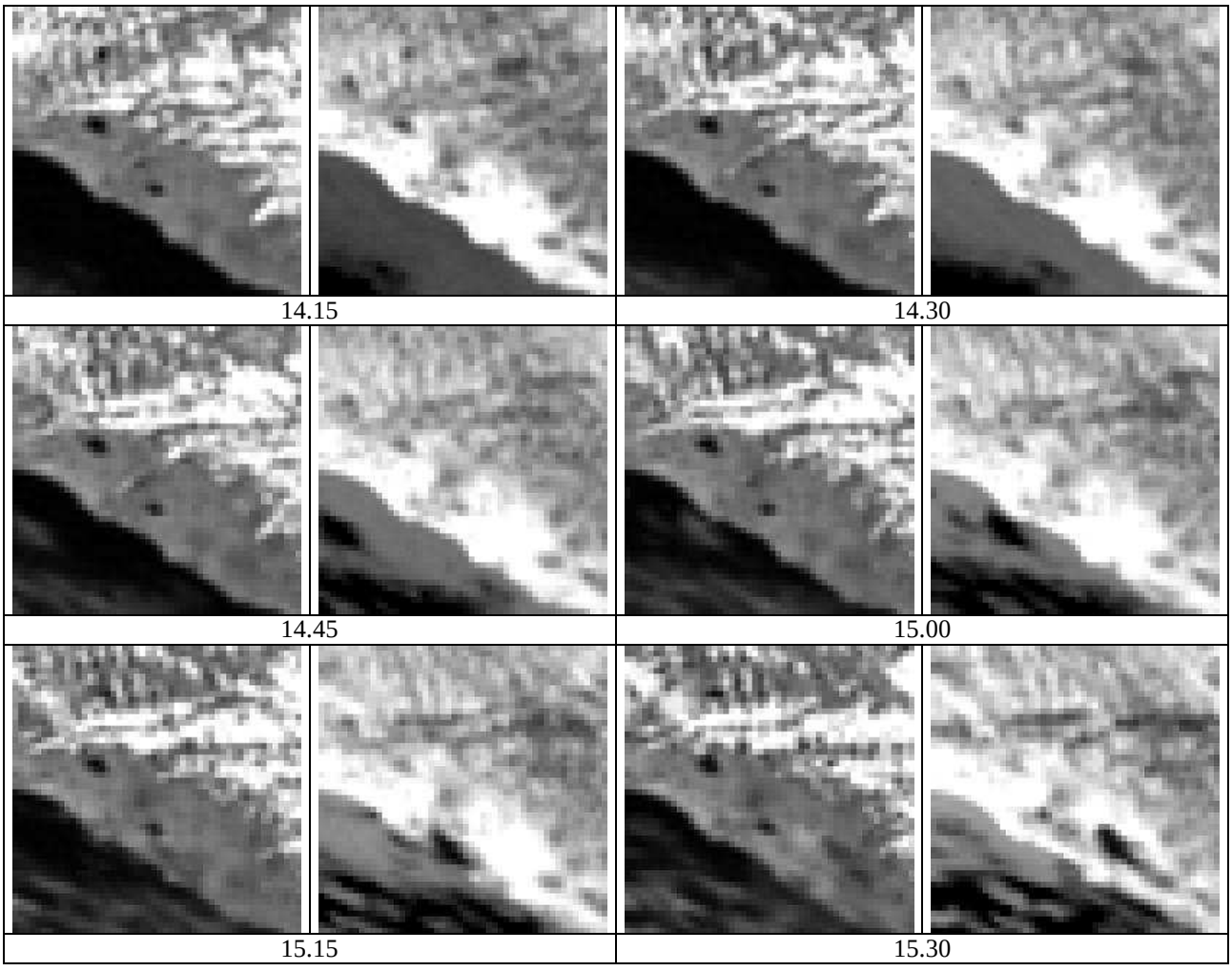

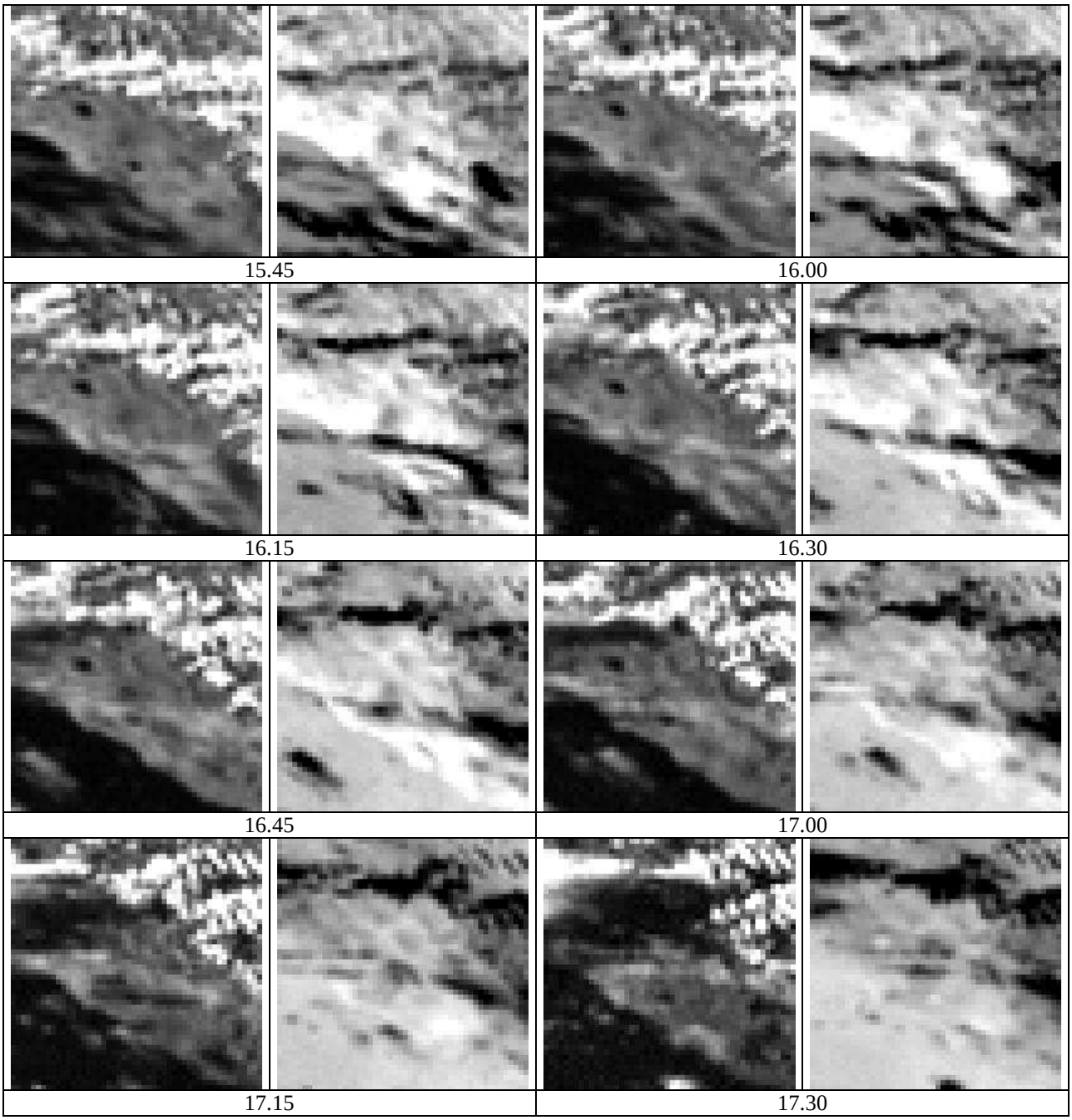

It can be affirmed that there is no evidence of pixels emerging for intensity respect to background. However, the retrieving process has been applied, but it produced no results. In fact, it can be noticed that clouds affect the scene of interest since 15.30 and this fact strongly reflects in the application of the inverting process. This is because the procedure is based on calculating radiance differences between two consecutive images, but the presence of clouds brings shifts in radiance values that, in fact, do not correspond to temperature variations consequent to fire presence. This can be observed in next figure, that reports the MIR channel behaviour along time in a pixel taken in the region of interest.

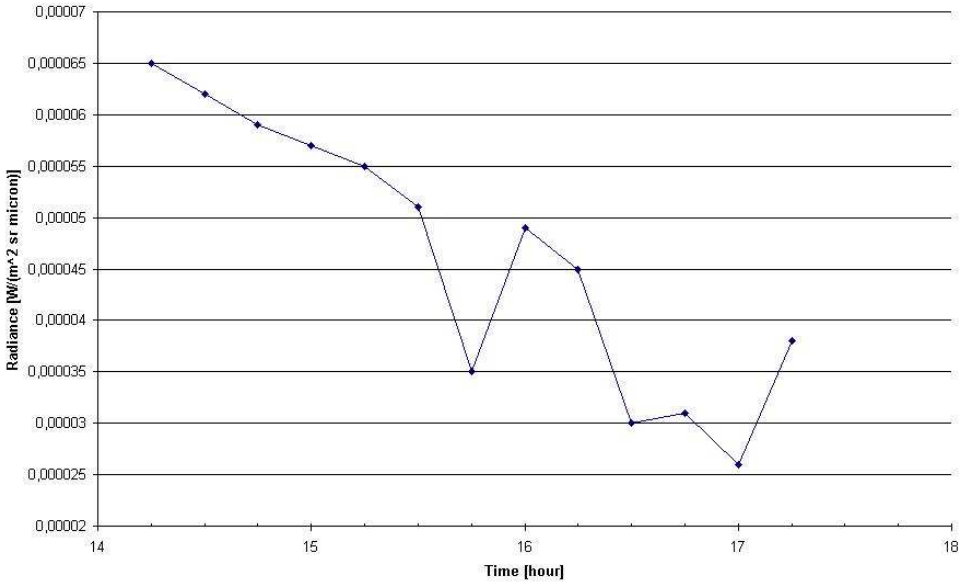

As a further element for the discussion, the AVHRR image mentioned in the previous section has been spatially resampled on MSG spatial resolution.

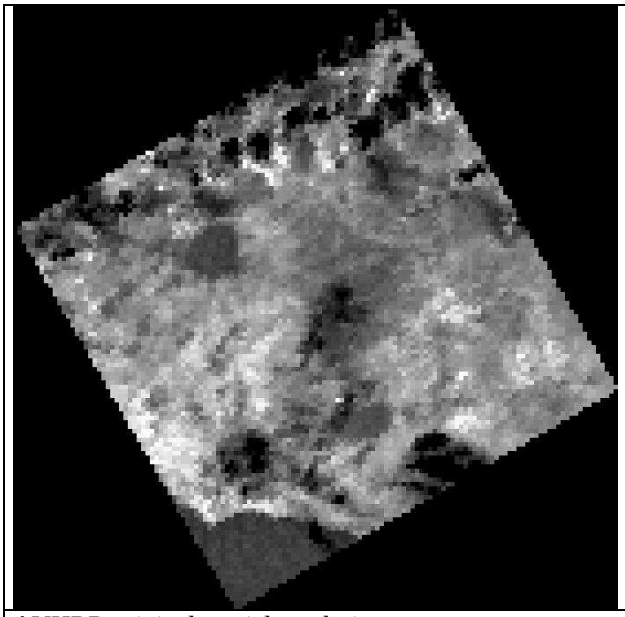

AVHRR original spatial resolution
(oriented according to MSG images)

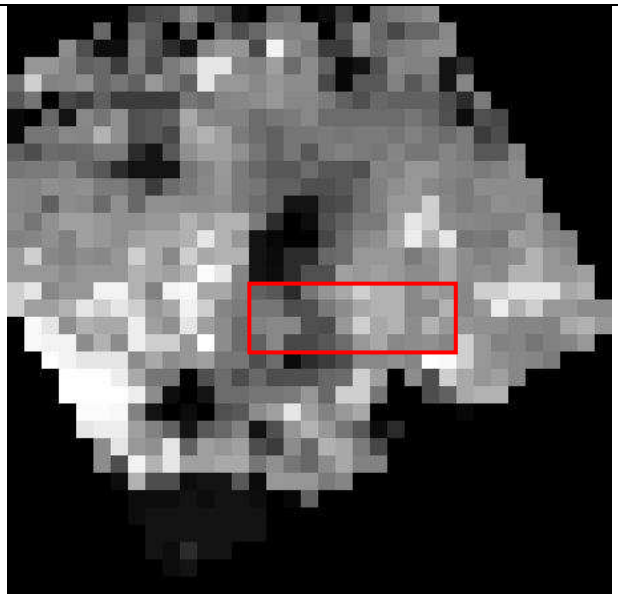

AVHRR resampled to MSG spatial resolution

As it can be seen in above figure, it is possible to identify in the resampled image some features present in the original one, but no more highlighted pixels are present in the area of interest as if the presence of fire is hidden from the background.

4.3 Comparison between airborn and satellite fire characterization map

4.3.1 Validation of Dozier bispectral method

Results obtained through satellite data, applying Dozier retrieval method, will be here validated comparing them to

information coming from HYPER data inversion.
Due to some uncertainty in the scale interpretation of calibrated images available for August 14th, the analysis will focus on radiant fractions computed with the presence of potassium peak in the spectrum.

As first step it was necessary to determine the extension of the area interested from the fire, so to compare it with the fraction retrieved in satellite data processing.
Taking the VNIR image for August 14th fire, the ratio between two bands (the potassio one and another next to it) have been computed over all the pixels.
Only those pixels with a ratio value greater than statistical fluctuations have been labelled as fire pixels and taken into account.

The resulting number of pixels in the Oriolo area is about 500 and their distribution is displayed in figure.

VNIR image

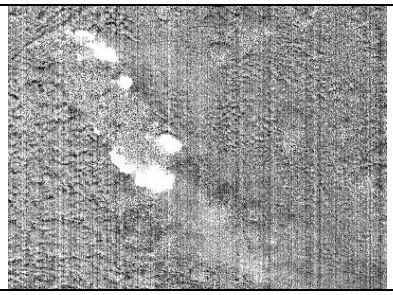

Band ratio
(768.76 nm / 780.39 nm)

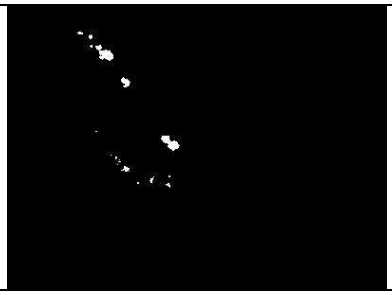

Fire pixels

Looking at other elements present in the VNIR image (as for example domestic animals), it is possible to say that pixel size in VNIR is about 0.5 m, so AVHRR pixel could contain up to about 4.0 10^6 HYPER VNIR pixels.
Therefore the two fractions to be compared are:

HYPER derived fraction	AVHRR retrieved fraction
0.000125	0.0001

which are comparable.

The same procedure was performed on the Magliano/Campagnano fire. In this case the “fire” pixel are about 1900.

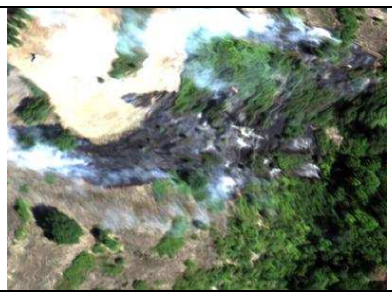

VNIR image

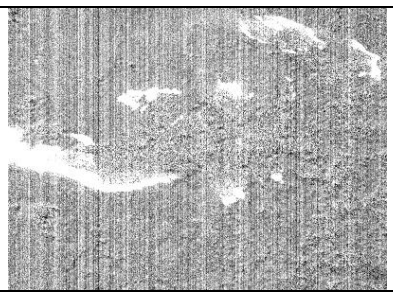

Band ratio
(768.76 nm / 780.39 nm)

Fire pixels

Before comparing numbers, it must be noted that this fire involves two adjacent radiant pixels in AVHRR image, so the HYPER derived fraction must be compared with the total of the two fraction retrieved from AVHRR pixels.

HYPER derived fraction	AVHRR retrieved fraction
0.000475	0.0002 + 0.00015

4.3.2 Satellite for detecting fire trace element : simulations

In this section we discuss on the different success rate of automatic fit of the function

$$F = fP(\lambda, T_1) + (1 - f)P(\lambda, T_2)$$

with respect to the number and wavelength of observable band in satellite observations. Assuming as input values for the parameters the following values:

T1	T2	fraction
1000 *K*	300 *K*	0.1
1000 *K*	300 *K*	0.01
1000 *K*	300 *K*	0.001
1000 *K*	300 *K*	0.0005
1000 *K*	300 *K*	0.0001

We run the fitting procedure for each of these configuration and register the minimum fraction which can be retrieved by the system. We obtain the following results:

Description	**Band1**	**Band2**	**Band3**	**Min fraction**	**Min fire detectable dimension**
AVHRR	3.74	10.8	12	10^{-4}	$100m^2$
MSG	1.6	3.9	12	10^{-5}	$\approx 100m^2$
SWIR ; MIR	1.6	3.9	-	$5 \cdot 10^{-5}$	$50m^2$
SWIR ; MIR	2.6	3.9		10^{-4}	$100m^2$
SWIR	1.6	2.6	-	10^{-5}	$10m^2$
TIR	-	12	13	$2 \cdot 10^{-4}$	$200m^2$

Table 4-1: *Minimum fire dimension observable with different configuration. The selected data set are shown in columns 'Band1, Band2, Band3', the column 'min fraction' contains the minimal fraction of pixel occupied by the fire, the column 'Min detectable fire dimension' contains the dimension in meters of the minimal fraction observable assuming a pixel size of 1Km. For the case of MSG satellite the pixel size is about 3 Km.*

After these simulations we conclude that:

- the AVHRR paylod permits to reach fraction of 10^{-4};
- MSG payload permits to reach fraction of 10^{-5} which corresponds to about the same dimension of AVHRR considering the different pixel size;
- SWIR bands seems the most useful in order to enhance the sensistivity of the system to small fires;
- the role of TIR seems to be marginal.

The vegetation reflected Sun radiation is expected to give a strong contribution in the SWIR bands. However this is true for low fire temperature and less true for high temperature fires. The addition of a MIR band help in retrieving small

fractions also in presence of strong vegetation reflected radiance. Anyway this contribution can be modeled and eliminated using theoretical atmosphere and vegetation models.

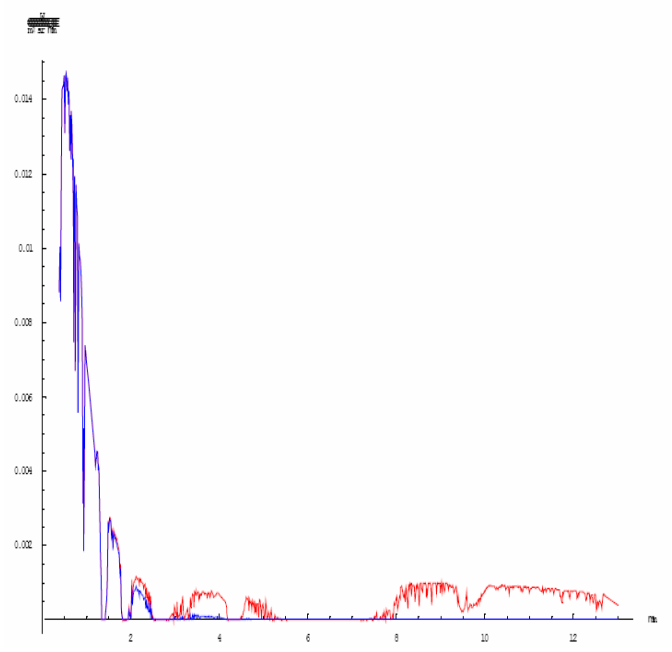

Blue line = sun reflected radiance
Red line = TOA radiance
T=800K

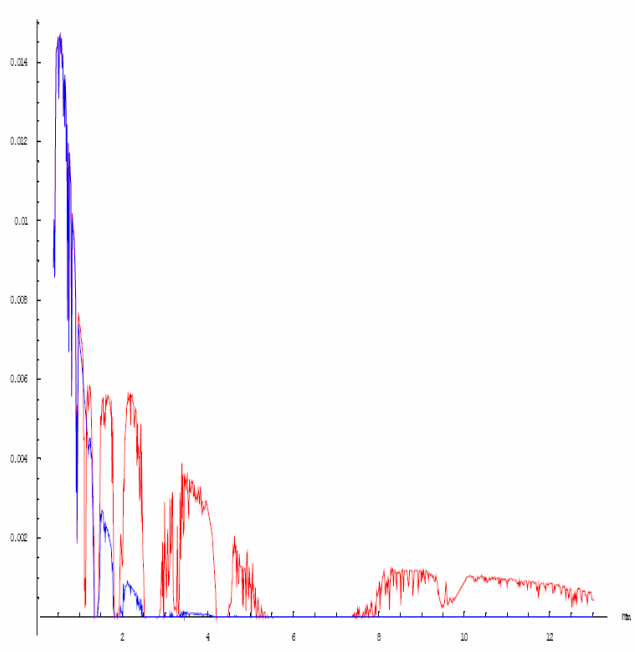

Blue line = sun reflected radiance
Red line = TOA radiance
T=1200K

Figure 4-2: *Modtran simulations of the different contribution of sun reflected radiance and emitted radiance from a pixel covered for a fraction of 0.5 % by fire*

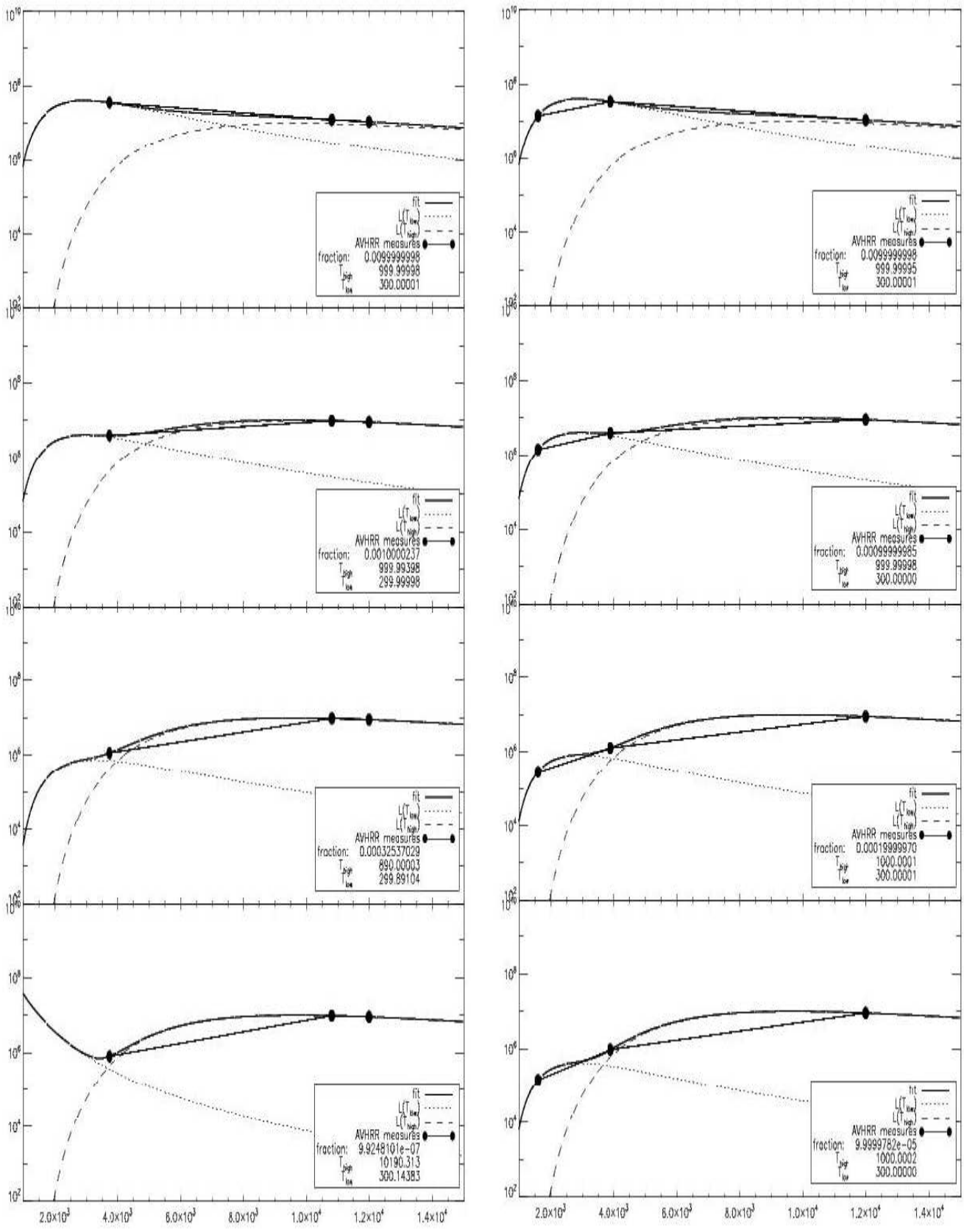

AVHRR MSG

Figure 4-3: *Two band configuration. Without TIR the detection of also small fraction is possibile***.**

4.3.3 Hyper and Hyperion comparison

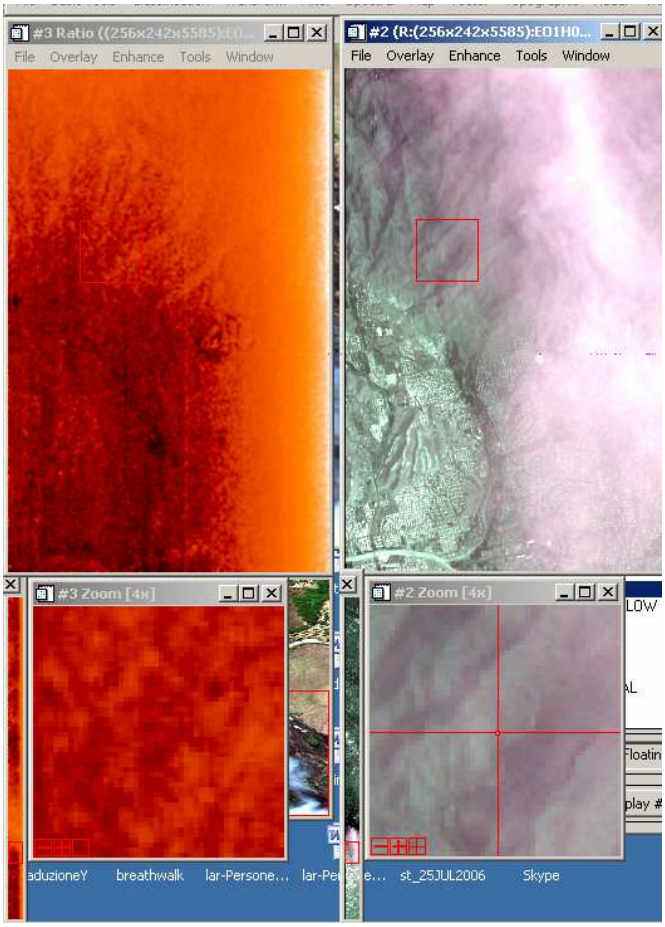

Discussion on usability SWIR VNIR observation for fire observation compared with satellite data

VNIR range

Using

- Hyperion with it's 10 nm resolution doesn't allow to distinguish the K doublet (766,5 and 769,9 nm). The band ratio technique doesn't allow to retrieve flaming area under the smoke.
- The two spectra are respectively an Hyperion in correspondence of a source and an hyper in correspondence of a source during the fire of 19 August 2006.

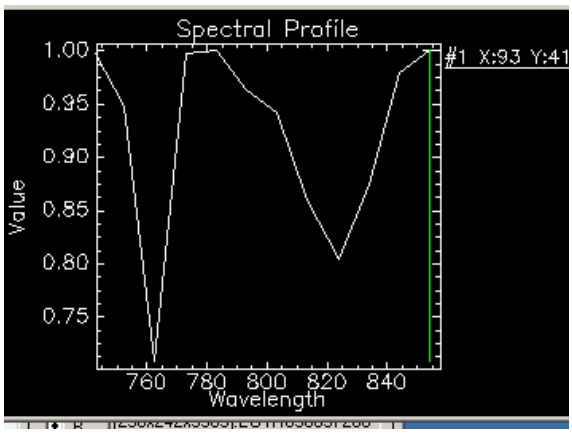

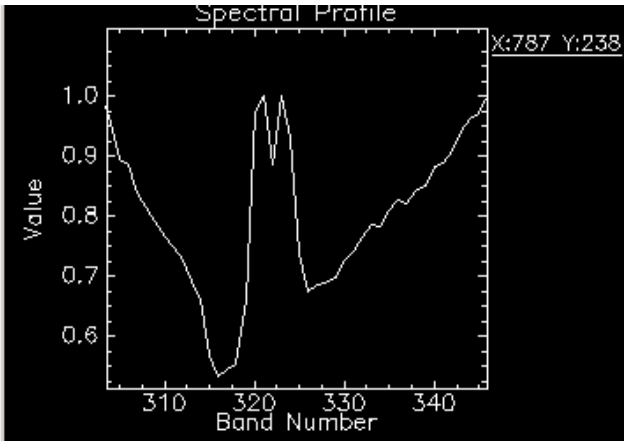

The band ratio applied to Hyperion data don't give any useful info while band ratio to Hyper data identifies the sources under the smoke

SWIR range

The **SWIR** Hyperion image shows clearly the front of fire and the active burning sources. The Hyper analysis in the almost same bands shows the front of fire. The image is rather noisy and with some saturation problem.

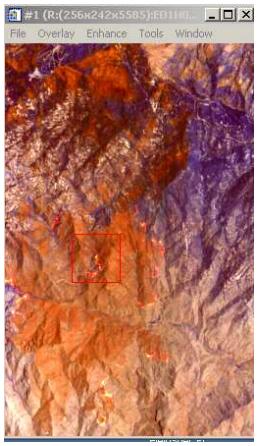

R=2224nm,
G=1568nm
B=1245 nm

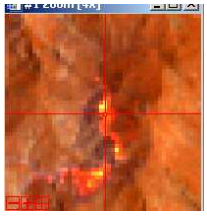

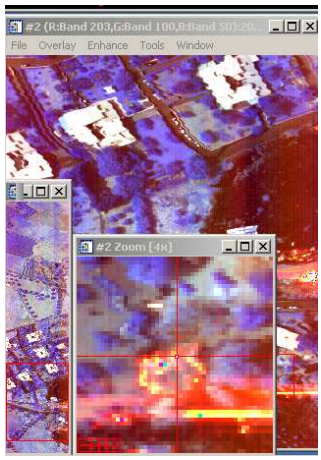

R=2221nm
G=1565nm,
B=1249nm

Spectral comparison

The radiance data of satellite and airborne systems were processed and compared after continuum removing. Spectrally we can find good agreement with position of absorbing bands.

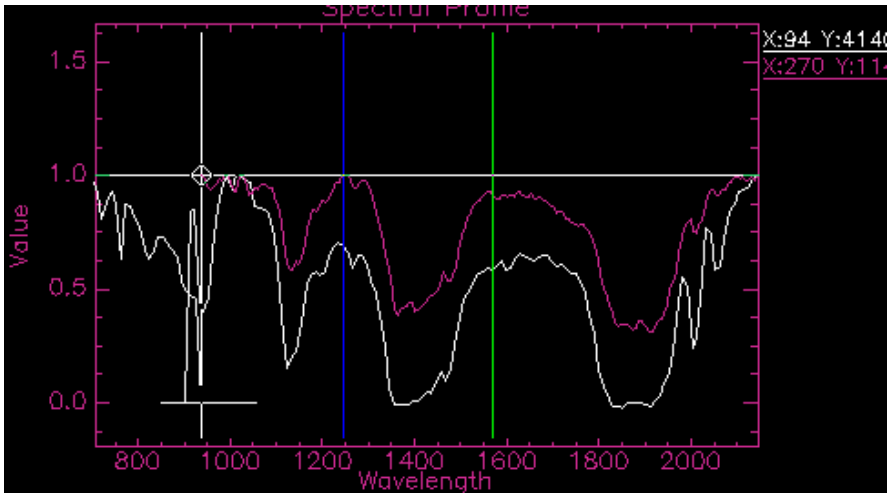

White Hyperion
Pink Hyper

5 Conclusions

This document reports on results obtained from the fires observational campaign performed during summer 2006 dedicated to the study of fire emission in the spectral region VNIR-SWIR.

Obtained results of the campaign have been:

- Realization of an hyperspectral data set containing data from fires in summer 2006 in Toscana an Lazio.
- Data set of ground measurement of vegetation
- validation of the hypothesis of using K line emission to trace firing regions
- develop of functions for fitting and studing fire emission.
- Comparison between fraction obtained with HYPER spectral observation (using K line method) and satellites derived (AVHRR) studies based on Dozier (Dozier et al 1981) method.
- Discussion on the minimal dimension of fires detectable for different payloads

Moreover in this project the behaviour of the HYPER instrument have been studied. In order to use the instrument as support for satellite observations, some improvements in the observational strategy and instrumental setup are required:

- the plane and platform motion must be more closely monitored in order to produce georeferenced images without post processing manual operations;
- strong saturation occurs in presence of fires. This effect cannot be eliminated only reducing the exposure time because the flux peak of a fire at temperature of 1000K is 10^9 times larger then the flux at a temperature of 300K.
  A selective filter which absorbs a large fraction of radiation at SWIR wavelength (where we expect the maximum of the flux emitted by the fire) and leave almost all the radiation in the VNIR, can be studied in a future work in order to improve the instrumental setup.

6 Appendix – data archive description

This document is intended primary to serve the community of scientists to enable data access and interpretation. In the following paragraph we show the data storage-data set description.

6.1 Data description

The data, acquired in fly by HYPER, are stored in ENVI standard format and have the following coding:

Filename: LLYYYMMDDTHHMMSS_cameraName_count. EXT where,

LL=level ID
YYY=year
MM= month
DD= days
T=separator
HH= hour
MM=minutes
SS=seconds
cameraName=VNIR, SWIR, VNIR_DARK, SWIR_DARK
count=0,1,2 etc.
EXT= is the extension of the file (e.g. for the data in Envi format ext is .hdr and . raw)

6.1.1 Data processing level number

The data set collected during the campaign are related by observation type, target, or time. The data set contains data of one processing level; the data of a different processing level will be treated as different data set.

DATA LEVEL NUMBER

Level	Proc. Type	Data Processing Level Description
0	Raw Data	telemetry with data embeded
1	Calibrated Data	data value are expressed in or are proportional to some physical Unit as radiance.
2	Resized Data	Data that have been resampled in the time or in the space Domains
3	Correlative data	Other science Data needed to interpret the dataset
4	User Description	Description of why the data were required and enough documentation to allow secondary user to extract information from data

2.0 Data Set Description

The Level 0 data (VIS and SWIR) are the data set acquired in four different fires. The data are in raw format as

acquired by the instrument. The header file (.hdr) contains all ancillary information about sample, bands, integration time, wavelength range. Also corresponding dark current data acquired on flight are provided in the same format.

Level 1 data are respectively a VIS and SWIR cube calibrated by Galileo Avionica (GA)by using laboratory calibration factors and laboratory dark current. This data set was chosen by GA due to low saturation level.

Level 2 data is the resized data set centered on the fire.

Level 3 ancillary measures.

In the table we summarize the selected data set:

HYPER Data SET

Filename	**Ancillary information**	**Vegetation type**
L0_20060804T134250_SWIR_.hdr L0_20060804T134250_SWIR_0.raw L0_20060804T134250_VNIR_1.raw L0_20060804T134250_VNIR_1.hdr	August 4 2006 Campagnano village	Bushes
L0_20060814T173443_SWIR_DARK_0.raw L0_20060814T173443_SWIR_DARK_0.hdr L0_20060814T173443_VNIR_DARK_0.hdr L0_20060814T173443_VNIR_DARK_0.raw L0_20060814T173642_SWIR_0.hdr L0_20060814T173642_SWIR_0.raw L0_20060814T173642_VNIR_1.hdr L0_20060814T173642_VNIR_1.raw	August 14 2006, Oriolo Village 42° 09′ 25.118″ – 12° 27′ 58. Lat 42° 11′ 28.329″ – Lon12° 08′ 47.061″293	Broad-leaved woods
L0_20060816T163841_SWIR_DARK_0.hdr L0_20060816T163841_SWIR_DARK_0.raw L0_20060816T163841_VNIR_DARK_0.hdr L0_20060816T163841_VNIR_DARK_0.raw L0_060816T165552_SWIR_0.hdr L0_060816T165552_SWIR_0.raw L0_20060816T165551_VNIR_0.hdr L0_20060816T165551_VNIR_0.raw	August 16 2006 Nemi village Lat 41° 43′ 17.121″ – Lon 12° 42′ 15.237″	Broad-leaved woods
L0_20060819T152504_SWIR_DARK_0.hdr L0_20060819T152504_SWIR_DARK_0.raw L0_20060819T152504_VNIR_DARK_0.hdr L0_20060819T152504_VNIR_DARK_0.raw L0_20060819T152718_SWIR_0.hdr L0_20060819T152718_SWIR_0.raw L0_20060819T152718_VNIR_1.hdr L0_20060819T152718_VNIR_1.raw	August 19 2006, Cerveteri Village, Lat 42° 00′ 13.125″ – Lon 12° 05′ 12.53″	Orchards and and cropped fields
L1_20060804T134250_SWIR_0_rad.raw L1_20060804T134250_SWIR__rad.hdr	August 4 2006 Radiance= data value*10^6(W/nm m^2 nmsr s-1)	
L2_20060814T173642_SWIR_0.raw L2_20060814T173642_SWIR_0.hdr L2_20060814T173642_VNIR_1.hdr L2_20060814T173642_VNIR_1.raw	Resized data set, August 14 2006, Oriolo Village 42° 09′ 25.118″ – 12° 27′ 58.	

2.1 Units of Measure

```
L2_20060816T165552_SWIR_0.hdr      Resized data set,
L2_20060816T165552_SWIR_0.raw
L2_20060816T165551_VNIR_0.hdr      August 16 2006
L2_20060816T165551_VNIR_0.raw      Nemi village
                                   Lat    41° 43’ 17.121” –
                                   Lon 12° 42’ 15.237”


L2_20060819T152718_SWIR_0_.hdr     Resized data set,
L2_20060819T152718_SWIR_0_.raw     August 19 2006,
L2_20060819T152718_VNIR_1_rad.hdr  Cerveteri Village,
L2_20060819T152718_VNIR_1_rad.raw  Lat  42°  00’  13.125”  –
                                   Lon 12° 05’ 12.53”

L3_20060824_ASH.000           Ground measurement taken
…                             in     Campagnano     for
L3_20060824_ASH.059           different surfaces.
L3_20060824_GRASS.000
…
L3_20060824_GRASS.059
L3_20060824_WOOD.000
…
L3_20060824_WOOD.112
```

The used units used in the dataset are the following

Quantity	Name of Unit	Symbol
Lenght	Meter	m
wavelenght	nanometer	nm
time	millisecond	msec
Power	Watt	W
Solid angle	Steradian	sr
radiance		10 6(W/nm m2 nmsr s)

Glossary

VNIR= visible near infrared channel of HYPER
GA = Galileo Avionica